Send Orders for Reprints to reprints@benthamscience.net

Current Medicinal Chemistry, 2025, *32*, 4259-4283

RESEARCH ARTICLE

Exploring Novel Quinoline-1,3,4-Oxadiazole Derivatives for Alzheimer's Disease: Their Design, Synthesis, and *In-Vitro* and *In-Silico* Investigations

Sana Saffour[1,*], Asaf Evrim Evren[1,2], Begüm Nurpelin Saglik[1] and Leyla Yurttas[1]

[1]*Department of Pharmaceutical Chemistry, Faculty of Pharmacy, Anadolu University, 26470, Eskişehir, Türkiye;* [2]*Department of Pharmacy, Vocational School of Health Services, Bilecik Seyh Edebali University, Bilecik, 11000, Türkiye*

ARTICLE HISTORY

Received: May 25, 2024
Revised: July 01, 2024
Accepted: July 08, 2024

DOI:
10.2174/0109298673333159240815061359

Abstract: ***Introduction*:** Alzheimer's Disease (AD) is a complicated and advanced neurodegenerative condition accompanied by gradual cholinergic neuronal death and higher levels of monoamine oxidase-B (MAO-B) enzyme. In this study, a series of novel hybrid compounds combining 1,3,4-oxadiazole and quinoline moieties were synthesized and evaluated for their potential as inhibitors of acetylcholinesterase (AChE), butyrylcholinesterase (BuChE), and MAO enzymes.

***Methods*:** The chemical structures of the synthesized compounds were confirmed using various analytical techniques, such as mass spectrometry, infrared spectroscopy (IR), proton nuclear magnetic resonance (1H-NMR), and carbon and nuclear magnetic resonance (13C-NMR). The final products were evaluated for anticholinesterase potential by applying modified Ellman's spectrometric method, whereas a fluorometric method was used to assess MAO inhibition properties. *In-silico* studies using molecular docking and molecular dynamics simulation (MDS) methods has been also conducted.

***Results*:** Among the synthesized compounds, 5a, 5c, and 6a demonstrated substantial activity against AChE, with IC_{50} values of 0.033 µM, 0.096 µM, and 0.177 µM, respectively. A molecular docking study was performed to elucidate the binding modes and establish the structure-activity relationship (SAR) of the most active compounds (5a, 5c, and 6a). Molecular dynamics simulation (MDS) of the most potent compound, 5a, was also conducted to examine the stability of the interactions with the receptor. Moreover, the physicochemical properties of the active products were also studied.

***Conclusion*:** Overall, this research contributes to the development of 1,3,4-oxadiazole-quinoline hybrids as potential AChE inhibitors for the treatment of Alzheimer's disease.

Keywords: 1,3,4-oxadiazole, quinoline, Alzheimer's disease, anticholinesterase, molecular docking, β-amyloid plaques.

1. INTRODUCTION

Alzheimer's Disease (AD) is a gradually worsening neurodegenerative disorder recognized for its impact on the aging population. It is primarily distinguished by the accumulations of atypical β-amyloid plaques, the formation of intraneuronal neurofibrillary tangles (NFTs), and the loss of neurons [1]. Extensive endeavors have been dedicated to elucidating the fundamental neuropathological mechanisms underlying these pathological alterations [2].

A widely accepted proposal is the cholinergic hypothesis, which highlights the significant impairment of cholinergic pathways that play a vital role in neural function, learning, and brain plasticity. The primary cholinergic neurotransmitter, acetylcholine (ACh), undergoes hydrolysis by acetylcholinesterase (AChE) in-

*Address correspondence to this author at the Department of Pharmaceutical Chemistry, Faculty of Pharmacy, Anadolu University, 26470, Eskişehir, Türkiye; E-mail: sanasaffour@anadolu.edu.tr

to choline and acetic acid, thereby regulating the levels of acetylcholine in the brain. However, in individuals with Alzheimer's disease, there is a noticeable reduction in acetylcholine levels within synaptic gaps due to an accelerated degradation rate of acetylcholine and degeneration of cholinergic neurons [3]. Consequently, this leads to the termination of synaptic transmission between neurons. The deficiency of acetylcholine is thus responsible for memory loss, learning deficits, and cognitive function deterioration associated with Alzheimer's disease [4].

In addition, the loss of cholinergic neurons has a significant impact on other aspects of the disease, exacerbating the progressive accumulation of Aβ (β-amyloid) plaques, inflammation, and oxidative stress. As a result, acetylcholinesterase inhibitors are commonly utilized as the primary pharmacological interventions in order to restore acetylcholine levels. This approach provides symptomatic relief for Alzheimer's disease, aiming to alleviate the cognitive impairments associated with the condition [5].

Another significant cholinesterase enzyme is butyrylcholinesterase (BuChE), whose activity has been observed to increase progressively in the advanced stages of AD, eventually becoming the primary enzyme responsible for breaking down acetylcholine [6]. Moreover, several studies have demonstrated that inhibitors of BuChE can impede the formation and aggregation of amyloid-beta fibrils [7]. Hence, medications that target both AChE and BuChE are anticipated to provide superior therapeutic advantages, leading to improved cognitive function [8, 9]. Numerous investigations have been conducted to create highly effective analogs of anticholinesterase [10, 11].

Currently, the pharmacological options available for the management of Alzheimer's disease include cholinesterase inhibitors, namely donepezil, rivastigmine, and galantamine, as shown in Fig. (**1**). These medications function by increasing the levels of acetylcholine and are typically prescribed for individuals with mild to moderate cases of the disease. Additionally, as an adjunctive therapy alongside cholinesterase inhibitors, the *N*-methyl-d-aspartate receptor (NMDAR) inhibitor memantine is commonly utilized in moderate cases of AD [12].

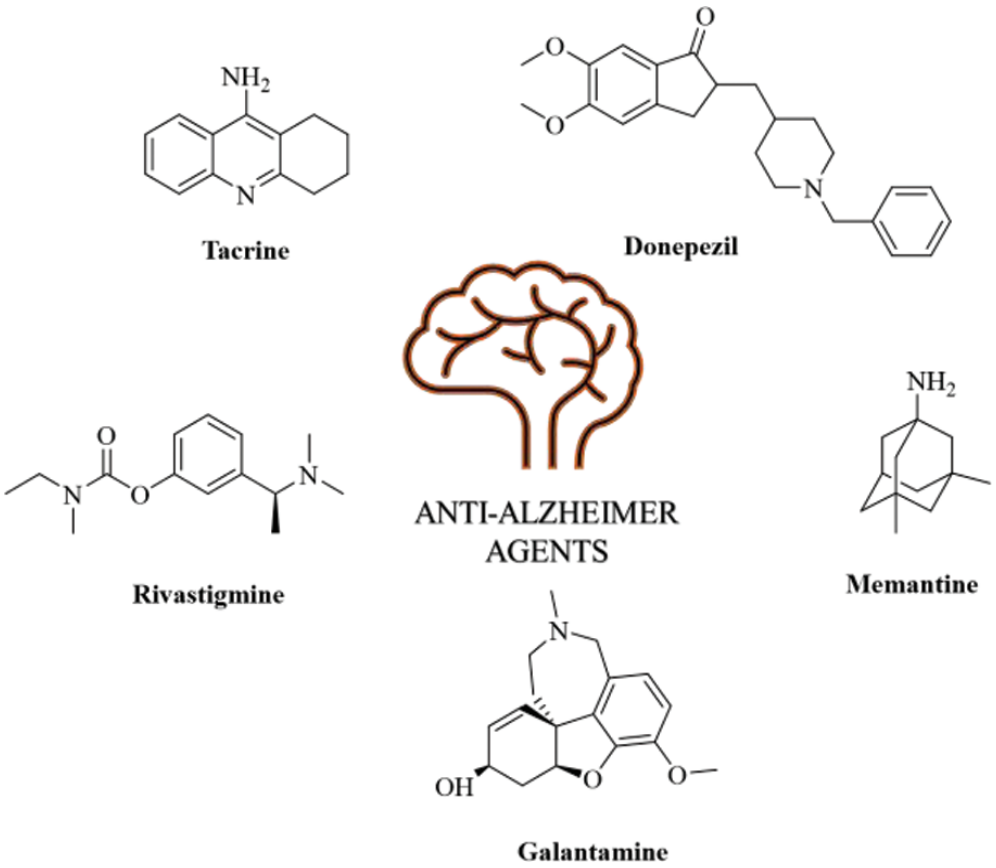

Fig. (1). Anti-Alzheimer's agents. (*A higher resolution / colour version of this figure is available in the electronic copy of the article*).

In 2021, the first disease-modifying immunotherapy known as aducanumab received approval for the treatment of mild cognitive impairment or mild Alzheimer's disease. Aducanumab is purported to function by targeting and eliminating abnormal beta-amyloid plaques in the brain, with the intention of reducing their overall quantity. However, the extent to which this drug effectively decelerates the progression of cognitive function impairment remains uncertain [13].

Furthermore, it has been observed that monoamine oxidase-B (MAO-B) is upregulated in the brains of individuals with Alzheimer's disease, and its activity is significantly increased, up to three-fold, particularly in brain regions associated with plaques, notably in astrocytes. In an attempt to impede the neurodegenerative process associated with Alzheimer's disease, several MAO-B inhibitors, including selegiline, rasagiline, and lazabemide, have been utilized. These inhibitors aim to exert neuroprotective effects through various mechanisms [14-16].

AChE active site is mainly composed of two main binding regions, namely peripheral anionic site (PAS) and catalytic active site (CAS). Recent research has also provided evidence demonstrating the role of the PAS of acetylcholinesterase in regulating enzyme expression and facilitating the accumulation of amyloid plaques. Consequently, it is anticipated that enzyme inhibitors capable of interacting with the amino acids in the PAS would exert a mitigating effect on the deposition of amyloid plaques, thereby exhibiting neuroprotective properties. Current investigations have focused on the development of dual-binding site inhibitors that target both the CAS and PAS domains, with the aim of simultaneously preventing acetylcholine degradation and AChE-induced Aβ aggregation [6, 17].

So far, several studies have been carried out to prepare skeletons that have the ability to ameliorate AD by dual inhibition of cholinesterase and MAO-B enzymes aiming to increase the efficiency of the compounds as anti-Alzheimer's agents [18].

The need for the development of multi-target agents has led researchers to explore the design of heterocycle-based compounds for the production of effective drugs targeting Alzheimer's disease. Extensive literature indicates that numerous heterocyclic compounds exhibit notable anti-Alzheimer's activity, suggesting their potential in the development of novel therapeutic agents for the disease [19].

One of the most important heptacyclic cores that have been used in the course of design and synthesis of medicinal agents is the 1,3,4-oxadiazole ring due to its wide range of chemical and biological properties [20, 21]. 1,3,4-Oxadiazole derivatives have exhibited exceptional potential in modulating Alzheimer's disease through multiple pathways. For example, certain derivatives have demonstrated a neuroprotective effect against toxicity induced by Aβ (amyloid-beta) [22]. Other compounds have shown inhibitory activity against glycogen synthase kinase-3β (GSK-3β), leading to a reduction in tau hyperphosphorylation and β-amyloid production. Furthermore, it has been established that numerous 1,3,4-oxadiazole derivatives possess anticholinesterase activity, which plays a critical role in Alzheimer's disease [22-26]. Additionally, several studies have demonstrated the ability of 1,3,4-oxadiazole derivatives to inhibit MAO enzymes [27, 28]. In 2019, Sharma *et al.* designed, synthesized, and tested a series of *N*-benzylpiperidine -1,3,4-oxadiazole multitargeted hybrids for Alzheimer's disease (Fig. **2I**). Several hybrids have displayed significant acetylcholinesterase (AChE), butyrylcholinesterase (BChE), and beta-secretase-1 (BACE-1) inhibition properties, as well as antioxidant properties [29].

In another study, Choubey *et al.* (2021) incorporated 1,3,4-oxadiazole and *N*-benzylpyrrolidine in the same skeleton and evaluated their potential to inhibit AChE, BChE, and BACE-1 enzymes (Fig. **2II**). Some derivatives demonstrated a remarkable potential to ameliorate cognitive dysfunction in *in-vivo* animal models [26].

Furthermore, 1,3,4-oxadiazole has been combined with ferulic acid in a single backbone and derivatized and then screened for AChE, BChE, and BACE-1 inhibition properties (Fig. **2III**). Numerous derivatives were found to have multifunctional inhibitory potential with significant IC_{50s} against these enzymes [25].

Another intriguing and fundamental heterocyclic core is quinoline, which has garnered significant interest in medicinal chemistry, particularly within the realm of heterocyclic compounds. This is primarily attributed to their broad spectrum of pharmacological activities, including anti-AD properties [30-34]. Furthermore, extensive research has been conducted on the quinoline core due to its known biological activity in inhibiting anticholinesterase and MAO, indicating its potential as a promising pharmacophore for the pathogenesis related to Alzheimer's disease [10, 32-37].

In 2021, Ziab *et al.* prepared a series of quinoline-thiosemicarbazone compounds and evaluated their cholinesterase inhibitory activities. One of the derivatives showed a highly potent anticholinesterase activity (Fig. **2IV**) [38]. Moreover, some coumarin-quinoline

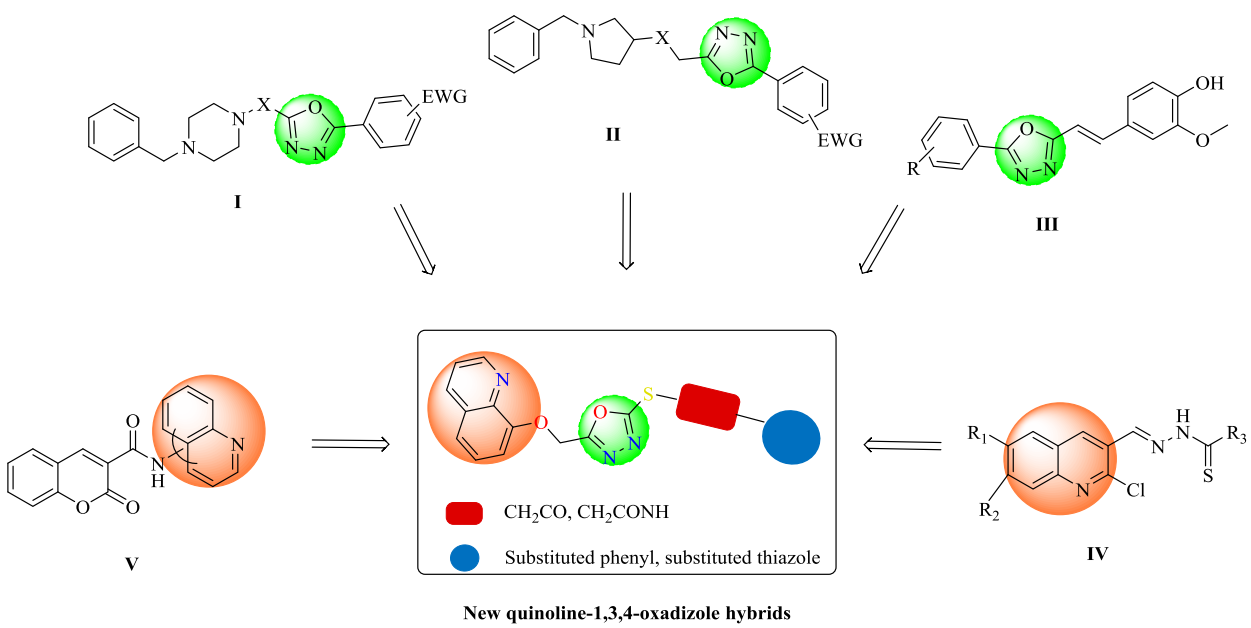

Fig. (2). Some quinoline and 1,3,4-oxadiazole hybrids with anti-Alzheimer's properties. (*A higher resolution / colour version of this figure is available in the electronic copy of the article*).

hybrids were produced, and *in-vitro* studies were conducted on their anticholinesterase and iron-chelating properties (Fig. **2V**) [39].

The objective of this research was to produce a series of compounds incorporating quinoline and 1,3,4-oxadiazole cores in their molecular structure, with the aim of pursuing an improved therapeutic profile in the context of Alzheimer's disease. Specifically, the structures were designed to simultaneously target cholinesterase and monoamine oxidase enzymes in order to target multiple pathways. Additionally, this study aimed to conduct *in-silico* analysis using molecular docking techniques to predict and analyze the binding interactions between the most active candidates and their respective target receptors.

2. MATERIALS AND METHODS

2.1. Chemistry

The chemicals were purchased from Merck Chemicals (Merck KGaA, Darmstadt, Germany) and Sigma-Aldrich Chemical Co. (Sigma-Aldrich Corp., St. Louis, MO, USA). Melting points (m.p.) were uncorrected and measured using the MP90 digital melting point apparatus (Mettler Toledo, Ohio, USA). The reactions were controlled by thin-layer chromatography (TLC) using Silica Gel 60 F_{254} TLC plates (Merck KGaA, Darmstadt, Germany). The mobile phase of TLC was petroleum ether-ethyl acetate (9:1, 3:1, and 1:1). Shimadzu 8040 LC/MS/MS system (Shimadzu, Tokyo, Japan) was used to determine the mass spectra HRMS of final compounds. ^{1}H-NMR and ^{13}C-NMR data were obtained using NMR, Bruker DPX- 300 FT-NMR spectrometer (Bruker Bioscience, Billerica, MA, USA) in DMSO-d_6 as solvent. The data were expressed as chemical shifts or δ values (ppm) relative to the internal standard TMS, and coupling constants (*J*) were given in *Hz*.

2.1.1. Synthesis of Ethyl 2-(Quinolin-8-yloxy) Acetate (1)

8-Hydroxyquinoline (7.25 g, 0.05 mol) was dissolved with the base potassium carbonate (13.82 g, 0.1 mol) and stirred for 15 min, then ethyl bromoacetate (6.61 mL, 0.06 mol) was added to the reaction mixture and heated at reflux temperature for 2-3 hours in acetone (100 mL). After TLC analysis, the solvent was evaporated, and the product was washed, filtered out of the water, and dried [40].

2.1.2. Synthesis of 2-(Quinolin-8-yloxy) Acetohydrazide (2)

Ethyl 2-(quinolin-8-yloxy)acetate **(1)** (10.3 g, 0.047 mol) was stirred with hydrazine monohydrate 85%

(0.01 mol, 7.3 mL) in ethanol (250 mL) for 1 hour at room temperature. The reaction was controlled using TLC, and the solid product was filtered and recrystallized from ethanol [40].

2.1.3. Synthesis of 5-[(Quinolin-8-yloxy)Methyl] -1,3,4-Oxadiazole-2-thiol (3)

An ethoxide solution was prepared by dissolving 2.44g of KOH (0.043 mol) in 100 mL of absolute ethanol. To this basic solution, 2-(quinolin-8-yloxy)acetohydrazide **(2)** (9.27 g, 0.0432 mol) was added, followed by the gradual addition of CS_2 (5.1 mL, 0.085 mol) to the reaction. The resulting mixture was then refluxed for 5-6 hours. After the reaction completion, the mixture was slowly poured into iced water and acidified with aqueous HCl until the pH reached 5-6. The crude product was then filtered and dried [41].

2.1.4. Synthesis of 1-(Substituted Phenyl)-2-[[5-((Quinolin-8-yloxy)Methyl)-1,3,4-oxadiazol-2-yl]thio]ethan-1-one (4a-4d)

For this process, 0.5g (0.001 mol) of 5-[(quinolin-8-yloxy)methyl]-1,3,4-oxadiazole-2-thiol **(3)** was mixed with 0.001 mol of substituted phenacyl bromide (0.001 mol) in the presence of the base potassium carbonate (0.0015 mol) in acetone (20 mL) at ambient temperature. After the reaction completion, the solvent was evaporated, and the resulting product was washed with water, filtered, and dried [42].

2.1.4.1. 1-Phenyl-2-[[5-((Quinolin-8-yloxy)Methyl) -1,3,4-oxadiazol-2-yl]thio]ethan-1-one (4a)

Yield 73%, m.p.=110-111°C. **FTIR (ATR, cm^{-1}):** 3053 (aromatic C-H stretching), 2920-2960 (aliphatic C-H stretching), 1676 (C=O), 1500-1600 (N=C, C=C stretching), 1261 (aromatic C-O stretching, oxadiazole), 1172 (aliphatic C-O stretching), 1118 (monosubstituted benzene).

^{1}H-NMR: (400 MHz, DMSO-d_6, ppm) δ: 5.16 (2H, s, CO-CH_2), 5.60 (2H, s, O-CH_2), 7.36 (1H, dd, J_1= 7.74 , J_2=1.06 *Hz*, quinoline C_7-H),7.52 (1H, t, J= 8.04 *Hz,* phenyl C_4-H), 7.55-7.63 (4H, m, aromatic-H), 7.71 (1H, t, J=7.42 *Hz,* phenyl C_4-H), 8.02 (2H, d, J=7.12 *Hz,* phenyl $C_{2,5}$-H), 8.35 (1H, dd, J_1= 8.30 , J_2=1.70 Hz, quinoline C_4-H), 8.87 (1H, dd, J_1= 4.13 , J_2 =1.74 Hz, quinoline C_2-H).

^{13}C-NMR: (100 MHz, DMSO-d_6, ppm) δ*:* 41.10(S-CH_2), 60.89(O-CH_2), 111.94, 121.94, 122.53, 127.03, 128.91, 129.36, 129.61, 134.46, 135.45, 136.45, 140.135, 140.91, 153.35, 164.14, 165.05, 192.71(C=O).

HRMS (*m*/*z*): $[M+H]^+$ calculated for $C_{20}H_{15}N_3O_3S$: 378.0907; found: 378.0910.

2.1.4.2. 2-[[5-((Quinolin-8-yloxy)methyl)-1,3,4-oxadiazol-2-yl]thio]-1-(p-tolyl)ethan-1-one (4b)

Yield 64%, m.p.= 148-149°C. **FTIR (ATR, cm^{-1}):** 3053 (aromatic C-H stretching), 2848-2954 (aliphatic C-H stretching), 1674 (C=O stretching), 1602-1490 (C=N, C=C stretching), 1261 (C-O stretching, oxadiazole), 1165 (C-O stretching, ether), 1118 (1,4 disubstituted benzene).

^{1}HNMR: (400 MHz, DMSO-d_6, ppm) δ: 2.40 (3H, s, phenyl-CH_3), 5.11 (2H, s, CO-CH_2), 5.60 (2H, s, O-CH_2), 7.36 (1H, d, J=1.76 Hz, quinoline C_7-H), 7.52 (1H, t, J= 7.95 Hz, phenyl-H), 7.56-7.63 (3H, m, aromatic-H), 7.93 (2H, d, J=8.2 Hz, aromatic-H), 8.36 (1H, dd, J_1= 8.3, J_2=1.67 Hz, quinoline C_4-H), 8.95 (1H, dd, J_1= 4.12, J_2=1.7 Hz, quinoline C_2-H).

^{13}C-NMR: (100 MHz, DMSO-d_6, ppm) δ*:* 21.69 (CH_3), 41.10 (S-CH_2), 60.88 (O-CH_2), 111.97, 121.94, 122.53, 127.07, 129.02, 129.62, 129.89, 132.96, 136.55, 140.02, 145.05, 149.86, 153.30, 164.10, 165.09, 192.19(C=O).

HRMS (*m*/*z*): $[M+H]^+$ calculated for $C_{21}H_{17}N_3O_3S$: 392.1063; found: 392.1049.

2.1.4.3. 1-(4-Methoxyphenyl)-2-[[5-[(Quinolin-8-yloxy)Methyl)-1,3,4-oxadiazol-2-yl]thio]ethan-1-one (4c)

Yield 71%, m.p.=170-171°C. **FTIR (ATR, cm^{-1}):** 3010-3057 (aromatic C-H stretching), 2918-2848 (aliphatic C-H stretching), 1668 (C=O stretching), 1500-1595 (C=N, C=C stretching), 1257 (C-O stretching, oxadiazole), 1165 (C-O stretching, ether), 1107 (1,4 disubstituted benzene).

^{1}HNMR: (400 MHz, DMSO-d_6, ppm) δ: 3.86 (3H, s, O-CH_3), 5.09 (2H, s, CO-CH_2), 5.61 (2H, s, O-CH_2), 7.08 (2H, d, J=1.76 Hz, phenyl-H), 7.37 (1H, d, J= 6.93 Hz, quinoline C_7-H), 7.52-7.63 (3H, m, quinoline-H), 8.02 (2H, d, J=8.9 Hz, phenyl-H), 8.36 (1H, dd, J_1= 8.29 , J_2=1.50 Hz, quinoline C_4-H), 8.88 (1H, dd, J_1= 4.09 , J_2=1.58 Hz, quinoline C_2-H).

^{13}C-NMR: (100 MHz, DMSO-d_6, ppm) δ*:*40.91 (S-CH_2), 56.12 (O-CH_3), 60.91 (O-CH_2), 112.01, 114.57, 121.94, 122.53, 127.08, 128.30, 129.62, 131.34, 136.62, 139.96, 149.83, 153.28, 164.07, 164.21, 165.17, 190.98 (C=O).

HRMS (*m*/*z*): $[M+H]^+$ calculated for $C_{21}H_{17}N_3O_4S$:408.1013; found:408.1019.

2.1.4.4. 1-(2,5-Dimethoxyphenyl)-2-[[5-((Quinolin-8-yloxy)Methyl)-1,3,4-oxadiazol-2-yl] thio]ethan-1-one (4d)

Yield 69%, m.p.= 124-125°C. **FTIR (ATR, cm^{-1}):** 3000-3050 (aromatic C-H stretching), 2835-2937 (aliphatic C-H stretching), 1643 (C=O stretching), 1608 (C=N stretching), 1494 (C=C stretching), 1263 (C-O stretching, oxadiazole), 1157 (C-O stretching, ether).

^{1}HNMR: (400 MHz, DMSO-d_6, ppm) δ: 3.37 (3H, s, O-CH_3), 3.89 (3H, s, O-CH_3), 4.92 (2H, s, CO-CH_2), 5.60 (2H, s, O-CH_2), 7.19 -7.22 (2H, m, aromatic-H), 7.37 (1H, d, J_1= 7.7, J_2=1.02 Hz, quinoline C_7-H), 7.50-7.63 (4H, m, aromatic-H), 8.34 (1H, dd, J_1= 8.33, J_2=1.72 Hz, quinoline C_4-H), 8.87 (1H, dd, J_1= 4.14 , J_2=1.71 Hz, quinoline C_2-H).

^{13}C-NMR: (100 MHz, DMSO-d_6, ppm) δ:45.01 (S-CH_2), 56.04 (O-CH_3), 56.95 (O-CH_3), 60.91 (O-CH_2), 111.94, 114.15, 114.80, 121.81, 121.93, 122.51, 125.48, 127.01, 129.61, 136.44, 140.13, 149.89, 153.37, 153.47, 153.88, 164.06, 165.27, 192.64 (C=O).

HRMS (*m*/*z*): $[M+H]^+$ calculated for $C_{22}H_{19}N_3O_5S$:438.1118; found: 438.1119.

2.1.5. Synthesis of 2-Chloro-N-(Substituted)Acetamide

A solution of 2-chloro-*N*-(thiazol-2-yl/phenyl)acetamide (0.005 mol) was prepared in 20 mL of tetrahydrofuran (THF) along with triethylamine (TEA) (0.005 mol) at a temperature of 0-5°C. Subsequently, chloroacetyl chloride (0.006 mol) was added dropwise to the reaction mixture while continuously stirring for 1-2 hours. After the completion of the reaction, THF was evaporated, and the resulting precipitate was washed with distilled water and dried [43].

2.1.6. N-(4-Substituted phenyl)-2-[[5-((quinolin-8-yloxy)methyl)-1,3,4-oxadiazol-2-yl]thio]acetamide (5a-c)

A solution of 2-chloro-*N*-(substituted)acetamide (0.001 mol) in acetonitrile was slowly added dropwise to a solution containing 5-[(quinolin-8-yloxy)methyl]-1,3,4-oxadiazole-2-thiol (0.5 g, 0.001 mol) and NaOH (0.04 g, 0.001 mol) in acetonitrile (10 mL). The resulting mixture was refluxed for 10 hours. After refluxing, the solvent was evaporated, and the product was washed with brine water. Subsequently, the product was recrystallized from ethanol to obtain pure crystals [44].

2.1.6.1. N-(4-Chlorophenyl)-2-[[5-((quinolin-8-yloxy)methyl)-1,3,4-oxadiazol-2-yl]thio]acetamide (5a)

Yield= 79%, m.p.=182-183°C. **FTIR (ATR, cm^{-1}):** 3172-3207 (N-H stretching), 3051-3061 (aromatic C-H stretching), 2920-2978 (aliphatic C-H stretching), 1730 (C=O stretching),1662 (C=N stretching), 1490-1570 (C=C stretching), 1240 (C-O stretching, oxadiazole), 1087(C-O stretching, ether), 1116 (1,4 disubstituted benzene).

^{1}H-NMR: (400 MHz, DMSO-d_6, ppm)δ: 4.10 (2H, s, CO-CH_2), 4.75 (2H, s, O-CH_2), 7.30 (1H, d, J=7.67 Hz, aromatic-H), 7.36 (1H, d, J=8.86 Hz, quinoline C_7-H), 7.50-7.60 (6H, m, aromatic-H), 8.34-8.37 (1H, m, quinoline-H), 8.80-8.89 (1H, m, quinoline-H), 10.52 (1H, s, NH).

^{13}C-NMR: (100 MHz, DMSO-d_6, ppm)δ: 37.22 (S-CH_2), 56.49 (S-CH_2), 111.98, 121.20, 121.96, 122.51, 127.04, 127.69, 129.21, 136.44, 138.05, 140.14, 149.90, 153.37, 164.19, 165.07, 165.27 (C=O).

HRMS (*m*/*z*): $[M+H]^+$ calculated for $C_{20}H_{15}N_4O_3ClS$:427.0626; found: 427.0609.

2.1.6.2. N-(4-Fluorophenyl)-2-[[5-((quinolin-8-yloxy)methyl)-1,3,4-oxadiazol-2-yl]thio]acetamide (5b)

Yield= 87%, m.p.=182-183°C. **FTIR (ATR, cm^{-1}):** 3292-3122 (N-H stretching), 3066 (aromatic C-H stretching), 2976-2841 (aliphatic C-H stretching), 1707 (C=O stretching), 1618 (C=N stretching), 1544 (C=C stretching), 1228 (C-O stretching, oxadiazole), 1116 (1,4 disubstituted benzene).

^{1}H-NMR: (400 MHz, DMSO-d_6, ppm)δ: 3.92 (2H, s, CO-CH_2), 4.55 (2H, s, O-CH_2), 7.28-7.37 (4H, m, aromatic-H), 7.51-7.58 (4H, m, aromatic-H), 8.36 (1H, d, J=6.17 Hz, quinoline C_4-H), 8.77-8.80 (1H, m, quinoline C_4-H).

^{13}C-NMR: (100 MHz, DMSO-d_6, ppm)δ: 32.49 (S-CH_2), 51.04 (S-CH_2), 116.07, 116.29, 120.31, 122.45, 127.60, 129.19, 130.85, 132.53, 136.84, 139.80, 149.65, 172.05 (C=O).

HRMS (*m*/*z*): $[M+H]^+$ calculated for $C_{20}H_{15}N_4O_3FS$: 411.0922 ; found: 411.0916.

2.1.6.3. N-(4-Methoxyphenyl)-2-[[5-((quinolin-8-yloxy)methyl)-1,3,4-oxadiazol-2-yl]thio]acetamide (5c)

Yield= 74%, m.p.= 206-207°C. **FTIR (ATR, cm^{-1}):** 3251-3196 (N-H stretching), 3053 (aromatic C-

H stretching), 2954-2848 (aliphatic C-H stretching), 1674 (C=O stretching), 1620 (C=N stretching), 1556 (C=C stretching), 1244 (C-O stretching, oxadiazole), 1170 (C-O stretching, ether), 1029 (1,4 disubstituted benzene).

^{1}H-NMR: (400 MHz, DMSO-d_6, ppm)δ: 3.79 (3H, s, O-CH_3), 4.20 (2H, s, CO-CH_2), 4.85 (2H, s, O-CH_2), 7.03 (2H, d, *J*=8.9 Hz, phenyl $C_{3,5}$-H), 7.23 (2H, d, *J*=8.9 Hz, phenyl $C_{2,6}$-H), 7.29 (1H, d, *J*=7.44 Hz, quinoline C_7-H), 7.50-7.63 (3H, m, aromatic-H), 8.38 (1H, dd, J_1= 8.28, J_2=1.5 Hz, quinoline C_4-H), 8.95 (1H, dd, J_1= 4.12, J_2=1.5 Hz, quinoline C_2-H), 10.79 (1H, s, NH).

^{13}C-NMR: (100 MHz, DMSO-d_6, ppm)δ: 33.44 (S-CH_2), 55.84 (O-CH_3), 69.28 (O-CH_2), 113.00, 114.74, 121.20, 121.75, 122.54, 127.27, 127.82, 129.82, 136.64, 140.35, 150.01, 154.40, 159.58, 159.68, 164,59, 171.77 (C=O).

HRMS (*m*/*z*): $[M+H]^+$ calculated for $C_{21}H_{18}N_4O_4S$: 423.1122 ; found: 423.1122 .

2.1.7. N-(Substituted thiazol-2-yl)-2-[[5-((quinolin-8-yloxy)methyl)-1,3,4-oxadiazol-2-yl]thio]acetamide (6a-c)

2.1.7.1. N-(4,5-Dimethylthiazol-2-yl)-2-[[5-((quinolin-8-yloxy)methyl)-1,3,4-oxadiazol-2-yl]thio]acetamide (6a)

Yield= 83%, m.p.= 175-176°C. **FTIR (ATR, cm^{-1}):** 3153 (N-H stretching), 3045 (aromatic C-H stretching), 2918 (aliphatic C-H stretching), 1670 (C=O stretching), 1618-1500 (C=N, C=C stretching), 1253 (C-O stretching, oxadiazole), 1163 (C-O stretching, ether).

^{1}H-NMR: (400 MHz, DMSO-d_6, ppm)δ: 2.15 (3H, s, thiazole CH_3), 2.23 (3H, s, thiazole CH_3), 4.36 (2H, s, CO-CH_2), 5.60 (2H, s, O-CH_2), 7.36 (1H, d, *J*= 7.45 Hz, quinoline C_7-H), 7.50-7.63 (3H, m, aromatic-H), 8.35 (1H, d, *J*= 8.16 *Hz*, quinoline C_4-H), 8.87 (1H, d, *J*= 2.56 Hz, quinoline C_2-H), 12.27 (1H, s, NH).

^{13}C-NMR: (100 MHz, DMSO-d_6, ppm)δ: 10.81 (-CH_3), 14.68 (-CH_3), 35.93 (S-CH_2), 60.97 (O-CH_2), 112.02, 121.97, 122.49, 127.02, 129.61, 136.41, 140.15, 149.90, 153.37, 164.28, 164.82 (C=O).

HRMS (*m*/*z*): $[M+H]^+$ calculated for $C_{19}H_{17}N_5O_3S_2$:428.0846; found 428.0851.

2.1.7.2. Ethyl 4-methyl-2-[2-[(5-((quinolin-8-yloxy)methyl)-1,3,4-oxadiazol-2-yl)thio]acetamido]thiazole-5-carboxylate (6b)

Yield 88%, m.p.= 208-209°C. **FTIR (ATR, cm^{-1}):** 3145 (N-H stretching), 3062 (aromatic C-H stretching), 2985-2873 (aliphatic C-H stretching), 1693 (C=O stretching), 1622-1500 (C=N, C=C stretching), 1284 (C-O stretching, oxadiazole), 1166 (C-O stretching, ether).

^{1}H-NMR: (400 MHz, DMSO-d_6, ppm)δ: 1.27 (3H, t, *J* = 7.1 Hz, $\underline{CH_3}$-CH_2), 2.54 (3H, s, thiazole-CH3), 3.34 (2H, q, *J*=7.1, CH_3-$\underline{CH_2}$), 4.43 (2H, s, CO-CH_2), 5.60 (2H, s, O-CH_2), 7.36 (1H, dd, J_1= 7.7, J_2=1.03 Hz, quinoline C_7-H), 7.50-7.61 (3H, m, aromatic-H), 8.34 (1H, dd, J_1= 8.33 , J_2=1.68 Hz, quinoline C_4-H), 8.86 (1H, dd, J_1= 4.12 , J_2=1.71 Hz, quinoline C_2-H), 12.91 (1H, s, NH).

^{13}C-NMR: (100 MHz, DMSO-d_6, ppm)δ: 14.63($\underline{CH_3}$-CH_2), 17.44 (thiazole-$\underline{CH_3}$), 35.89 (S-CH_2), 60.93 (CH_3-$\underline{CH_2}$), 61.04 (O-CH_2), 111.96, 114.87, 121.95, 122.47, 127.00, 129.60, 136.40, 140.13, 149.87, 153.36, 162.42, 164.35, 166.60 (C=O).

HRMS (*m*/*z*): $[M+H]^+$ calculated for $C_{21}H_{19}N_5O_5S_2$: 486.0900 ; found: 486.0908.

2.1.7.3. N-(4-Phenylthiazol-2-yl)-2-[[5-((quinolin-8-yloxy)methyl)-1,3,4-oxadiazol-2-yl]thio]acetamide (6c)

Yield 86%, m.p.= 188-189°C. **FTIR (ATR, cm^{-1}):** 3128 (N-H stretching), 3062-3026 (aromatic C-H stretching), 2991-2848 (aliphatic C-H stretching), 1678 (C=O stretching), 1698-1562 (C=N, C=C stretching), 1236 (C-O stretching, oxadiazole), 1163 (C-O stretching, ether).

^{1}H-NMR: (400 MHz, DMSO-d_6, ppm)δ: 4.46 (2H, s, CO-CH_2), 5.61 (2H, s, O-CH_2), 7.33 (1H, t, *J*=7.28 Hz, aromatic-H), 7.37 (1H, d, *J*=7.64 Hz, quinoline C_7-H), 7.44 (2H, t, *J*=7.48 Hz, aromatic-H), 7.50-7.62 (3H, m, aromatic-H), 7.67 (1H, s, thiazole-H), 7.9 (2H, d, *J*=7.98, aromatic-H), 8.35 (1H, d, *J*=8.15 Hz, quinoline C_4-H), 8.87 (1H, d, *J*=3.97 Hz, Quinoline C_2-H), 12.75 (1H, s, NH).

^{13}C-NMR: (100 MHz, DMSO-d_6, ppm)δ: 35.89, 61.02, 108.91, 112.13, 121.99, 122.50, 126.15, 127.06, 128.33, 129.22, 129.62, 134.62, 136.55, 140.04, 149.45, 149.86, 149.86, 153.31, 158.03, 164.33, 164.80, 164.87 (C=O).

HRMS (*m*/*z*): $[M+H]^+$ calculated for $C_{23}H_{17}N_5O_3S_2$: 476.0846; found: 476.0805 (Figs. **S1-S40**).

2.2. Determination of Anticholinesterase Activity

The inhibitory activity of the synthesized products against acetylcholinesterase and butyrylcholinesterase was assessed using a modified Ellman's spectrometric method in 96-well plates. The pipetting processes were carried out using the Biotek Precision XS robotic system from Winooski, VT, USA. The inhibition percentages were measured at 412 nm using a BioTek-Synergy H1 microplate reader from Winooski, VT, USA. Prior to the analysis process, all solutions were equilibrated at 20-25°C. Each well of the 96-well plates contained a mixture comprising 140 µL of phosphate buffer (0.1 M, pH = 8), 20 µL of 5,5′-dithiobis-(2-nitrobenzoic acid) DTNB (0.01 M), 20 µL of enzyme solution acquired from electric eel AChE or equine serum BuChE in 1% gelatin solution (2.5 U/mL), 20 µL of the inhibitor solution prepared in 2% aqueous DMSO, and 10 µL of the substrate solution (0.075 M acetylthiocholine iodide (ATC) or butyrylthiocholine iodide (BTC)), resulting in a final volume of 210 µL in each well. A preliminary prescreening evaluation was conducted to assess the enzyme inhibitory activities, and the results were presented as percentages at concentrations of 10^{-3} M and 10^{-4} M. For the evaluation of acetylcholinesterase inhibitory activity, donepezil was tested as a reference drug. Furthermore, for the evaluation of butyrylcholinesterase inhibitory activity, tacrine was employed as a reference agent.

The enzyme-inhibitor solutions were prepared by adding the enzyme, inhibitor, and chromogenic reagent DTNB to the phosphate buffer and then incubating the mixture at 25°C for 15 minutes. Subsequently, the substrate solution of acetylthiocholine iodide (ATC) or butyrylthiocholine iodide (BTC) was poured into the mixture. The yellow color produced during the reaction was controlled by determining the absorbance at 412 nm for a duration of 5 minutes. Additionally, a control solution without the inhibitor was prepared for comparison. To obtain the corrected readings, the absorbance values of both the control and inhibitor samples were adjusted by subtracting the blank readings. The percentage inhibition (% inhibition) was then quantified using the following formula **(1)**.

$$\%\ inhibition = \frac{[(A(C)-A(B))-(A(I)-A(B))]}{(A(C)-A(B))} * 100 \qquad (1)$$

Blank (B): inhibitor and substrate-free well.

Control (C): inhibitor-free well.

A(B): The blank measurements absorbance difference.

A(C): The control measurements absorbance difference.

A(I): The inhibitor measurements absorbance difference.

Compounds that exhibited inhibition higher than 50% at a concentration of 10^{-4} M were further screened at lower concentrations from 10^{-5} M to 10^{-9} M. A dose-response curve was constructed using GraphPad Prism software (version 5.0) by plotting the percentage inhibition against the logarithm of the concentration. This curve allowed for the determination of the IC_{50} values, which represent the concentration of the compound prerequisite to decrease the enzyme activity by 50% [45, 46].

2.3. Determination of Monoamine Oxidase Inhibitory Activity

For the evaluation of MAO isoenzyme inhibition, the synthesized compounds were subjected to an *in-vitro* fluorometric method. Solutions of the inhibitors in 2% DMSO were prepared at concentrations of 10^{-3} M and 10^{-4} M. Additionally, recombinant human MAO-A (0.5 U/mL) and MAO-B (0.64 U/mL) enzymes were prepared in phosphate buffer. A working solution mixture consisting of horseradish peroxidase (200 U/mL, 100 µL), Ampliflu™ Red (20 mM, 200 µL), and tyramine (100 mM, 200 µL) in a solution of phosphate buffer was also prepared. All the volumes were adjusted to a definitive volume of 10 mL.

In the 96-well micro test plate, 20 µL of the inhibitor solution was introduced to each well, followed by the addition of 100 µL of *h*MAO-A or *h*MAO-B enzyme solution. The plate was then incubated for 30 minutes at 37°C. After the initial incubation, 100 µL of the working solution was added to each well, and the plate was incubated for an additional 30 minutes. Fluorescence measurements were taken at 5-minute intervals with excitation/emission wavelengths set at 535/587 nm. To investigate the potential inhibitory effect of the compounds on horseradish peroxidase, parallel testing proceeded using a 3% H_2O_2 solution (20 mM, 100 µL) instead of the enzyme solutions. To assess the possible non-enzymatic inhibition of the compounds, the inhibitor and working solutions were mixed separately [47, 48]. All experiments were conducted in quadruplicate, and the inhibition percentage was quantified by applying the following equation **(2).**

$$\%inhibition = \frac{(FC_{t2}-FC_{t1})-(FI_{t2}-FI_{t1})}{FC_{t2}-FC_{t1}} * 100 \qquad (2)$$

FC_{t2}: Fluorescence emitted by the control at t_2 time.

FC_{t1}: Fluorescence emitted by the control at t_1 time.

FI_{t2}: Fluorescence emitted by the inhibitor at t_2 time.

FI_{t1}: Fluorescence emitted by the inhibitor at t_1 time.

2.4. ADME Parameters

The pharmacokinetic profile and physicochemical characteristics of the active molecules were calculated using the SwissADME online tool. Parameters, such as the number of hydrogen-bond (H-bond) acceptors and donors, lipophilicity, blood-brain barrier permeability, topological polar surface area, and drug-likeness properties, were evaluated and compared to those of donepezil [49].

2.5. Molecular Docking

The binding modes of the most potent derivatives were determined through docking simulations using the crystal structure of human acetylcholinesterase (PDB ID: 4EY7) obtained from the Protein Data Bank (PDB). The crystal structure was optimized by removing water molecules, heteroatoms, and co-factors using the Protein Preparation Wizard protocol available in the Schrödinger Suite 2020. The ligands were optimized by assigning protonation states, bond orders, and atom types using the LigPrep module in Schrödinger Maestro. Prior to the docking runs, a grid was generated by applying the Glide module, and the docking was performed using the standard precision docking mode [50].

2.6. Molecular Dynamics Simulation

Molecular dynamics simulations are recognized as a crucial computational tool for assessing the time-dependent stability of ligand-receptor complexes. In this research, we conducted MDS simulations for a duration of 100 nanoseconds to ensure the stability of the most potent compound identified in the docking results. To achieve this, we utilized the Desmond application, employing the Schrodinger Suite's standard force field (OPLS3e) along with the transferable intermolecular potential with a 3-point (TIP3P) water model. The complex underwent an energy minimization process, and system neutralization was accomplished by introducing Na^+ and Cl^- ions. Additionally, 150 mM NaCl in the dynamic conditions was included. Following the setup of the system, molecular dynamics simulation was started using NPγT ensemble modified heat, which was 310.55 K as obtained for optimal body temperature. Key structural parameters, such as the radius of gyration (Rg), root mean square fluctuation (RMSF), and root mean square deviation (RMSD), were produced using the Desmond application [47, 51].

3. RESULTS AND DISCUSSION

3.1. Chemistry

The compounds discussed in the study share a common skeleton consisting of a 1,3,4-oxadiazole ring connected to a quinolin-8-yloxy methyl group at the 5th position. To generate different derivatives, modifications were made to the groups attached to the thiol group located at position 2 of the 1,3,4-oxadiazole ring.

The study yielded the final compounds through a four-step synthetic procedure represented in Scheme **1**. Initially, 8-hydroxyquinoline was combined with ethyl bromoacetate under basic conditions, resulting in the formation of a compound **(1)**. Subsequently, compound **(1)** was reacted with hydrazine monohydrate to generate an acylhydrazine **(2)**. The produced hydrazide was then cyclized into 1,3,4-oxadiazole **(3)** using carbon disulfide in an ethoxide solution. Finally, the final products were synthesized using two distinct substitution reaction (SN_2) methods (Table **1**). The first procedure took place at room temperature using potassium carbonate and acetone **(4a-4d)**, while the second procedure occurred at 100°C using sodium hydroxide and acetonitrile **(5a-5c**, **6a-6c).**

In the compounds that contained amide structures (**5a-5c**, **6a-6c**), an N-H band was observed in the range of 3100-3300 cm^{-1}, while the carbonyl group was detected in the range of 1670-1707 cm^{-1}. The stretching of sp^2 hybridized carbons with C-H bonds was observed above 3000 cm^{-1}, while the sp^3 hybridized carbons were identified in the region of 2885-2990 cm^{-1}. The signals occurring at 1228-1284 cm^{-1} indicated the aromatic C-O stretching of the oxadiazole ring. Additionally, peaks in the range of 1170-1000 cm^{-1} indicated the presence of aliphatic C-O bonds.

The samples were dissolved in DMSO-d_6, which appeared as a quintet at 2.5 ppm in all spectra. A strong singlet at approximately 3.34 ppm was observed in the spectra of all compounds, indicating the presence of water protons. Upon examining the ^{1}H-NMR spectra of the compounds, the C_7, C_4, and C_2 protons of the quinoline ring were identified as doublets or doublet of doublets within the respective ppm ranges of 7.29-7.45, 8.34-8.38, and 8.77-8.95 (Fig. **3**).

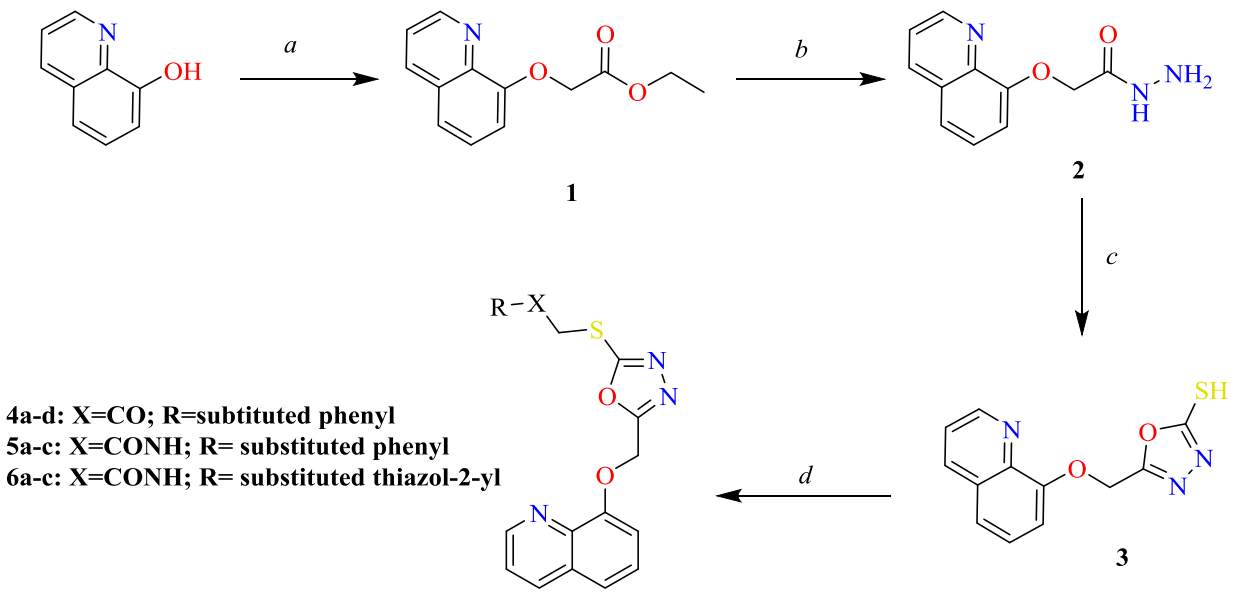

Scheme 1. Schematic representation of the synthetic pathways. Reaction conditions: (**a**) $CH_2BrCO_2C_2H_5$, K_2CO_3, acetone, reflux; (**b**) $NH_2NH_2.H_2O$, ethanol, r.t; (**c**) CS_2, KOH, ethanol, reflux; (**d**) substituted phenacyl bromides or 2-chloro-*N*-(substituted)thiazole/ phenylacetamide derivatives, base.

Table 1. The substitution of the final compounds.

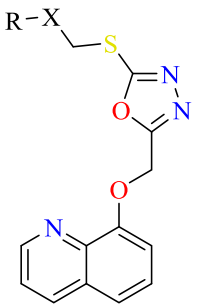

Compounds	X	R
4a	-CO-	phenyl
4b	-CO-	*p*-tolyl
4c	-CO-	4-methoxy phenyl
4d	-CO-	2,5-dimethoxy phenyl
5a	-CONH-	4-chloro phenyl
5b	-CONH-	4-fluoro phenyl
5c	-CONH-	4-methoxy phenyl
6a	-CONH-	4,5-dimethylthiazol-2-yl
6b	-CONH-	4-CH_3, 5-COOEt thiazol-2-yl
6c	-CONH-	4-phenylthiazol-2-yl

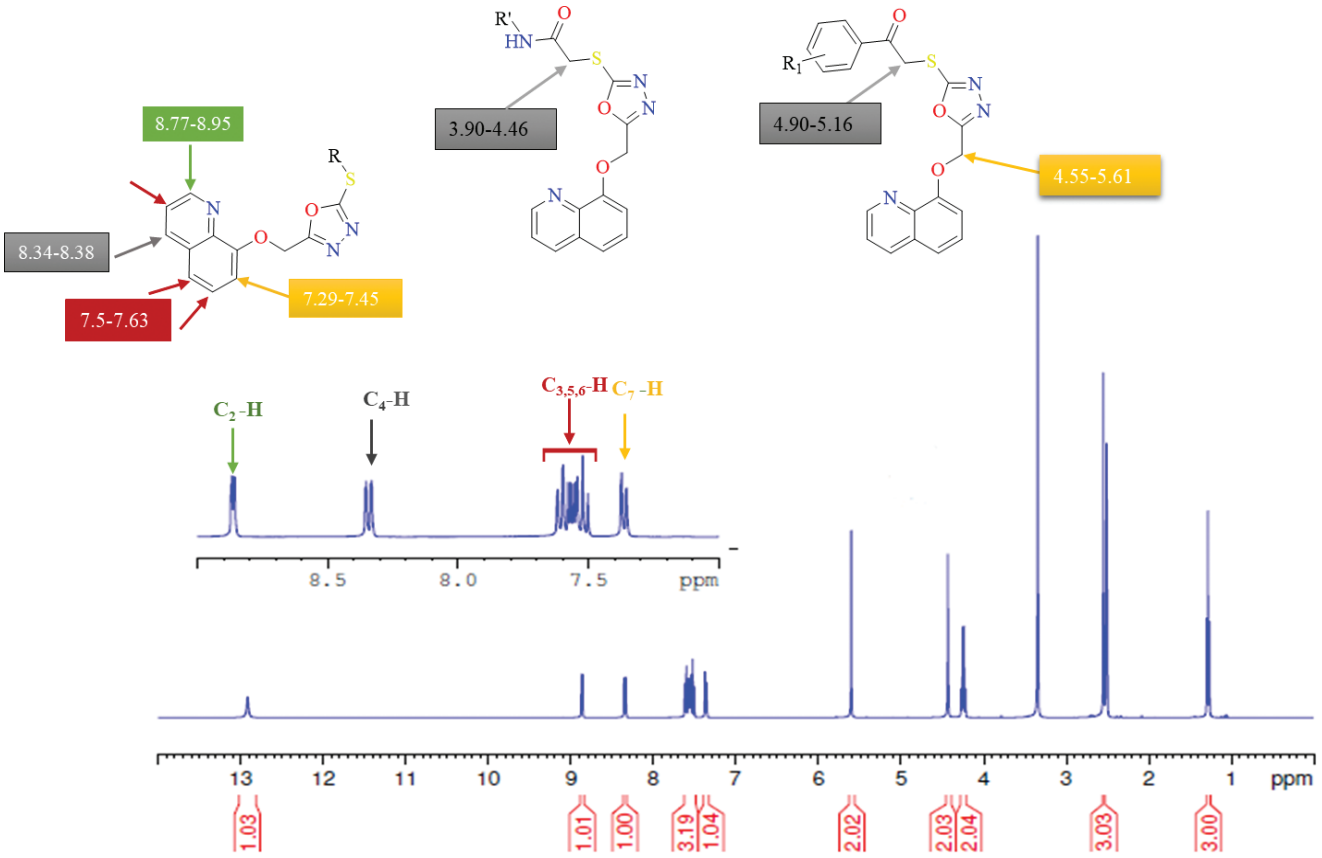

Fig. (3). [1]HNMR of quinoline -oxadiazole derivatives ranges (compound **6b** [1]NMR). (*A higher resolution / colour version of this figure is available in the electronic copy of the article*).

The C_3-H, C_5-H, and C_6-H protons were observed as multiplets within the range of 7.5-7.63 ppm. However, in structures containing substituted phenyl acetamide, the protons of the oxymethylene group connected to quinoline-C_8 appeared as singlets at 5.60-5.61 ppm. In substituted phenyl acetamide structures, the oxymethylene protons were detected as singlets in the range of 4.55-4.85 ppm. The protons of the methylene group attached to the phenyl acyl group in compounds **4a-4c** were detected as singlets within the range of 4.90-5.16 ppm. On the other hand, the methylene protons attached to the acetamide group were shielded and appeared at 3.90-4.46 ppm in compounds **5a-5c** and **6a-5c**. In compound **4b**, the phenyl-CH_3 protons were detected at 2.40 ppm as singlets. However, in compound **4c**, the methoxy protons were observed at a downfield position, considering the deshielding effect of the oxygen atom. In the ^{13}C-NMR spectra (Fig. **4**), the solvent peak appeared as a septet at approximately 39.95 ppm. Each sample required one hour for analysis. The chemical shifts of the oxymethylene carbon and thiomethylene carbon were observed in the upfield region, within the ranges of 56-70 ppm and 32-45 ppm, respectively. On the other hand, the carbonyl carbon was the most deshielded carbon in all compounds. In amide groups, the carbonyl carbon appeared in the range of 164-173 ppm, while in non-amidic structures, it was deshielded to 190-192 ppm. All aromatic carbons were observed within the range of 111-165 ppm. HRMS spectroscopy results of the compounds were found to be in good agreement with the calculated molecular weights of the compounds.

3.2. Anticholinesterases Activity Evaluation

All compounds in this study showed a higher inhibition profile against AChE compared to BuChE (Table **2**). With the exception of compound **4d**, all compounds displayed an inhibition percentage greater than 50% at a concentration of 10^{-3} M. An interesting observation is that all structures containing acetamide groups (**5a-5c** and **6a-6c**) exhibited inhibitory percentages higher than 75% at a concentration of 10^{-3} M for

AChE. Furthermore, when the concentrations were reduced to 10^{-4} M, compounds **5a, 5c**, and **6a** still demonstrated more than 80% inhibitory activity. Following the preliminary screening, compounds **5a**, **5c**, and **6a** were selected to determine their IC_{50} values for acetylcholinesterase. These compounds were tested at concentrations ranging from 10^{-5} to 10^{-9} M against AChE alongside the reference drug donepezil. The reference drug donepezil showed an IC_{50} value of 0.0201 µM while the IC_{50}s of compounds **5a**, **5c**, and **6a** were calculated as 0.033 µM, 0.096 µM, and 0.177 µM, respectively. These results indicate that compound **5a** exhibited the highest potency, followed by compound **5c**, while compound **6a** demonstrated slightly lower inhibitory activity against acetylcholinesterase.

The most potent compound in this series was **5a**, with an IC_{50} value of 0.033 µM. It had a 4-chlorophenylacetamide substitution connected by a thioether bridge to the fifth position of the 1,3,4-oxadiazole ring. Replacing the chlorine atom at the para position of compound **5a** with a methoxy group in compound **5c** resulted in a three-fold reduction in the inhibitory action, as indicated by the IC_{50} value of 0.096 µM. On the other hand, when the chlorine atom was replaced with a fluorine atom in compound **5b**, the inhibitory activity was found to be non-significant. Furthermore, substituting the 4-chlorophenyl acetamide group in compound **5a** with a 4,5-dimethylthiazole group in compound **6a** led to a decrease in inhibitory activity, with an IC_{50} value of 0.177 µM. It is important to note that other thiazole substitutions displayed relatively low activity compared to compound **6a**. The synthesized products, along with the reference tacrine, were tested on BuChE at concentrations of 10^{-3} M and 10^{-4} M. The results showed that compounds **5a**, **5c**, and **6a** exhibited enzyme inhibition of higher than 50% at the concentration of 10^{-3} M. However, when the concentrations were reduced to 10^{-4} M, the inhibition percentages were reduced to less than 35% for these compounds. Therefore, they were not further tested at lower concentrations.

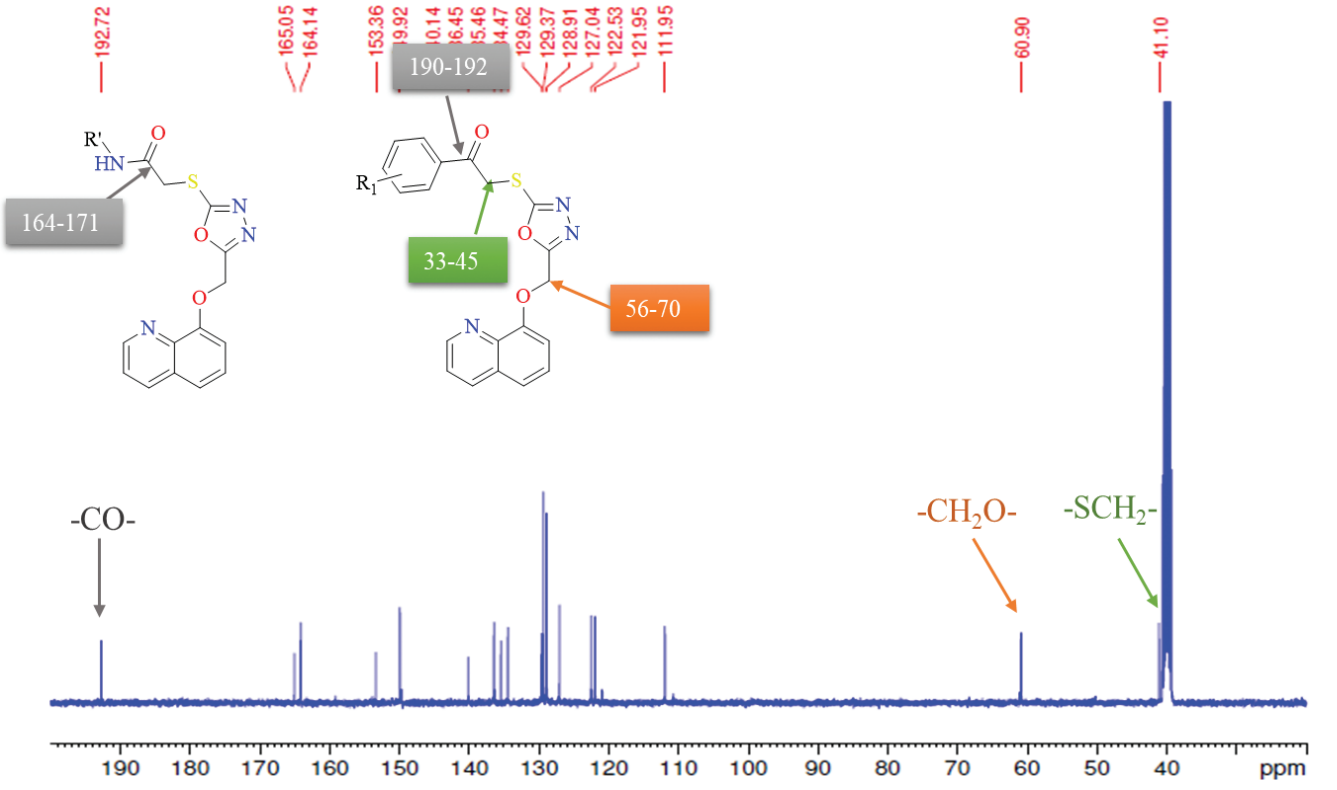

Fig. (4). ^{13}CNMR of quinoline -oxadiazole derivatives ranges (compound 6b 13CNMR). (*A higher resolution / colour version of this figure is available in the electronic copy of the article*).

Table 2. Inhibition results of the acetylcholinesterase and butyrylcholinesterase.

Code	AChE % Inhibition		AChE IC_{50} (µM)	BuChE % Inhibition		BuChE IC_{50} (µM)	Selectivity	SI*
	10^{-3} M	10^{-4} M		10^{-3} M	10^{-4} M			
4a	**66.532±1.267**	39.461 ±0.836	>100	25.821±0.832	20.611 ±0.754	>1000	AChE	>10
4b	**76.098 ±1.191**	41.690 ±1.234	>100	29.748 ±0.736	22.598 ±0.957	>1000	AChE	>10
4c	**64.562 ±0.937**	40.751 ±0.958	>100	22.830 ±0.961	18.448 ±0.884	>1000	AChE	>10
4d	42.837 ±1.022	37.828 ±0.877	>1000	32.454 ±0.827	27.962 ±0.997	>1000	-	-
5a	**94.662 ±1.654**	**90.709 ±2.136**	**0.033 ±0.001**	**61.088 ±0.903**	31.035 ±1.057	>100	AChE	>3030.303
5b	**81.769 ±2.036**	42.302 ±0.832	>100	30.320 ±1.155	21.219 ±0.763	>1000	AChE	>10
5c	**93.952 ±1.788**	**87.276 ±1.923**	**0.096 ±0.004**	**57.464 ±0.869**	23.892 ±0.747	>100	AChE	>1041.667
6a	**88.312 ±2.228**	**82.065 ±1.045**	**0.177 ±0.007**	**54.615 ±0.641**	20.464 ±0.957	>100	AChE	>564.97
6b	**79.406 ±1.455**	39.467 ±0.799	>100	33.934 ±0.825	29.657 ±0.873	>1000	AChE	>10
6c	**83.823 ±1.058**	47.975 ±0.817	>100	32.162 ±1.288	27.338 ±0.930	>1000	AChE	>10
Donepezil	99.156 ±1.302	97.395 ±1.255	0.0201 ±0.0010	-	-	-	AChE	-
Tacrine	-	-	-	99.827 ±1.378	98.651 ±1.402	0.0064 ±0.0002	BuChE	-

Abbreviations: *SI: selectivity Index (SI=IC_{50} BuChE/ IC_{50} AChE).

3.3. Monoamine Oxidases Inhibition Evaluation

The final compounds were screened for their inhibitory activities against MAO isoenzymes using the 10-acetyl-3,7-dihydroxyphenoxazine (Amplex Red™) assay. This assay relies on the oxidation of Amplex Red to the fluorescent compound resorufin by horseradish peroxidase and H_2O_2. At a concentration of 10^{-3} M, the screening results for MAO-A inhibition showed inhibition percentages ranging from 26% to 39% when compared to the reference inhibitors moclobemide (94%) and clorgyline (96%). For MAO-B inhibition, the range was between 30% and 48% at the same concentration. Upon reducing the concentrations to 10^{-4} M, the inhibition percentages against MAO-A and MAO-B decreased to 20-31% and 20-35%, respectively. Consequently, further investigations at lower concentrations were omitted due to the weak inhibitory action of the compounds. The results are displayed in Table **3.**

3.4. ADME Parameters

The physicochemical descriptors, pharmacokinetic properties, and medicinal chemistry friendliness of the most potent structures were determined using the SwissADME online tool. The log *p* values, which indicate the lipophilicity *via* the partition coefficient between octanol and water, were found to be 3.52 for **5a**, 2.99 for **5c**, and 3.12 for **6a**. Compounds **5a** and **5c** were predicted to have a high gastrointestinal absorption ability, indicating good bioavailability. However, the thiazole-containing structure **6a** had lower bioavailability. All active structures had 6 or 7 hydrogen bond acceptors (HBA) and only one hydrogen bond donor (HBD). Structures **5a** and **5c** exhibited no deviation from Lipinski, Ghose, Veber, Egan, and Muegge's rules, which indicate drug-likeness properties. However, structure **6a** deviated from these rules due to its high TPSA.

The prediction of the physicochemical parameters for the active compounds and the reference drug donepezil are illustrated in Table **4**.

Table 3. % inhibition of the prepared molecules against MAO-A and MAO-B enzymes.

Compound	MAO-A % Inhibition		MAO-B % Inhibition	
	10^{-3} M	10^{-4} M	10^{-3} M	10^{-4} M
4a	29.421±0.922	23.751±0.732	41.787±0.933	29.361±0.836
4b	38.911±0.949	20.248±0.857	45.408±1.275	30.733±0.920
4c	26.308±0.758	22.812±0.790	40.967±1.098	35.964±1.154
4d	30.134±0.836	20.435±0.846	48.048±1.348	31.012±0.830
5a	37.875±0.902	31.928±1.128	31.855±0.862	27.457±0.764
5b	30.590±0.777	27.116±0.875	36.223±0.935	20.628±0.622
5c	27.056±0.859	23.564±0.836	30.714±0.914	26.267±0.875
6a	39.621±0.921	31.355±1.044	40.695±1.262	33.018±1.091
6b	31.764±0.720	27.486±0.751	46.414±1.146	30.126±0.861
6c	35.599±1.246	29.804±0.880	43.768±1.451	28.430±0.728
Moclobemide	94.121±2.760	82.143±2.691	-	-
Clorgyline	96.940± 1.250	91.308± 1.305	-	-
Selegiline	-	-	98.258±1.052	96.107±1.165

Table 4. *In-silico* physicochemical properties of the active compounds.

	MW (g/mol)	HBA	HBD	TPSA (Å^2)	Log P	GI abs.	DL	BBB perm.
5a	426.88	6	1	115.44	3.52	High	5/5	No
5c	422.46	7	1	124.67	2.99	High	5/5	No
6a	427.50	7	1	156.57	3.12	Low	2/5	No
Donepezil	379.49	4	0	38.77	4.00	High	5/5	Yes

Abbreviations: MW, molecular weight; HBA, the number of hydrogen bond acceptor; HBD, the number of hydrogen bond donor; TPSA, the topological polar surface area; Log *P*, partition coefficient (Consensus Log $P_{o/w}$); GI abs, gastrointestinal absorption; DL, drug-likeness (including Lipinski, Ghose, Veber, Egan, and Muegge's rules); BBB perm., the Blood-Brain Barrier permeability.

3.5. Molecular Docking

This study utilized a high-resolution crystal structure (with a resolution of 2.35 Å) of human acetylcholinesterase co-crystallized with donepezil (PDB ID: *4EY7*) as the basis for conducting the molecular modeling investigation [50].

The findings obtained from the molecular docking investigation of compound **5a** with acetylcholinesterase (AChE) revealed the occurrence of five π-π interactions between **5a** and AChE. Notably, three of these interactions were observed between the quinoline ring of the ligand and Trp286 situated in the peripheral anionic site (PAS) region, while the remaining two π-π interactions occurred between the phenyl ring of the ligand and Trp86 within the CAS of the enzyme (Fig. **5**).

Additionally, the compound demonstrated two halogen interactions, wherein the chloro-substitution in the ligand engaged with Tyr133 and Gly120 in AChE. Moreover, two ar-H (aromatic hydrogen) interactions were observed in the 3D model representation (Fig. **6**). The first ar-H interaction took place between quinoline C_3-H of the ligand and Ser293 in the enzyme, while the second ar-H interaction was identified between the oxygen in the ether bridge of the ligand and Tyr341 in AChE.

Blue carbons: compound **5a**; white carbons: binding site residues; cyan dashes: aromatic H-bond; blue dashes: π-π interaction; purple dashes: halogen interaction.

Compound **5c** exhibited five π-π interactions in the molecular docking study. Specifically, two of these interactions occurred between the quinoline ring of the ligand and Trp86 in the active site. Additionally, the oxadiazole ring of the compound engaged in two π-π stacking interactions with Tyr337 and Tyr341, while another π-π stacking interaction was distinguished between the phenyl ring of the ligand and Trp286 (Fig. **7**).

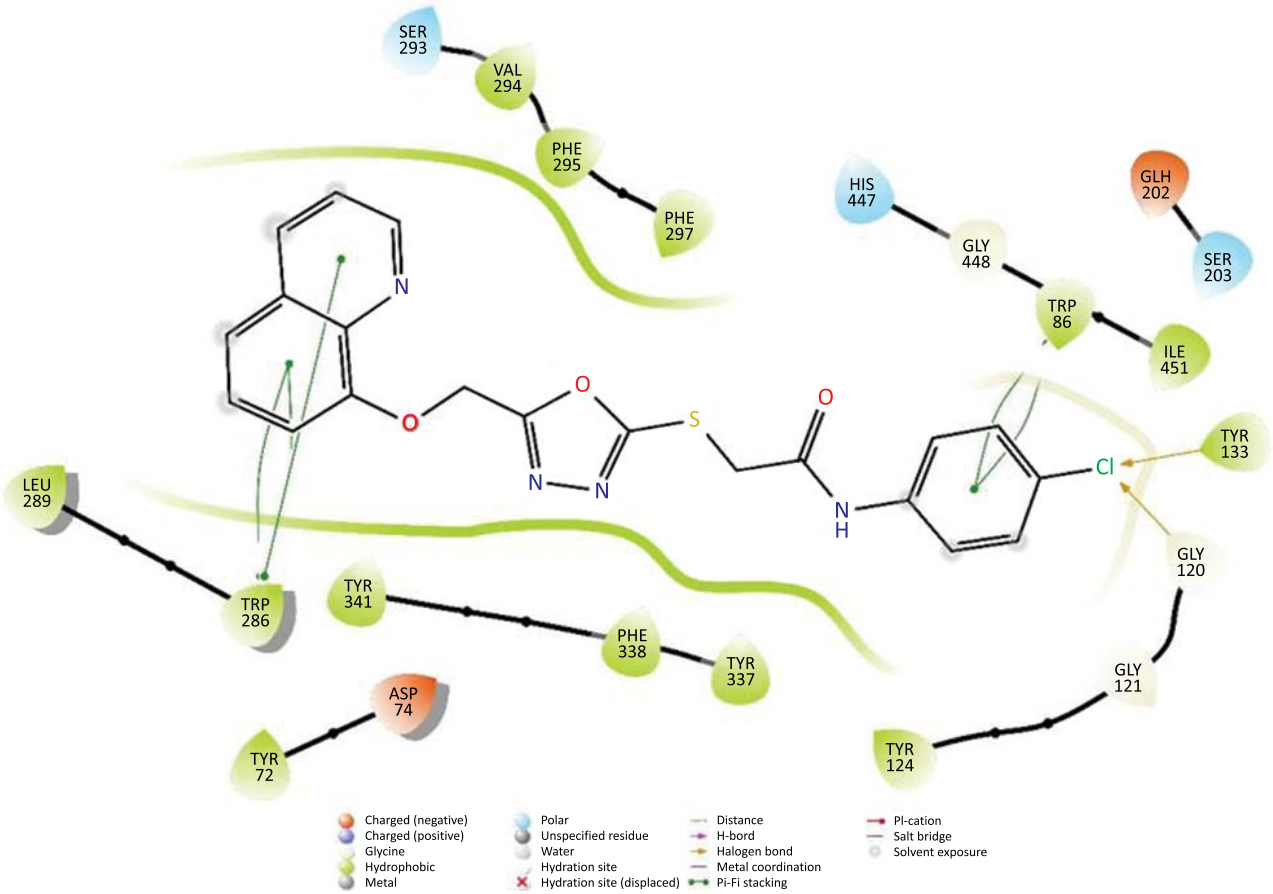

Fig. (5). 2D interactions of compound **5a** at the binding region (PBDID: 4EY7). (*A higher resolution / colour version of this figure is available in the electronic copy of the article*).

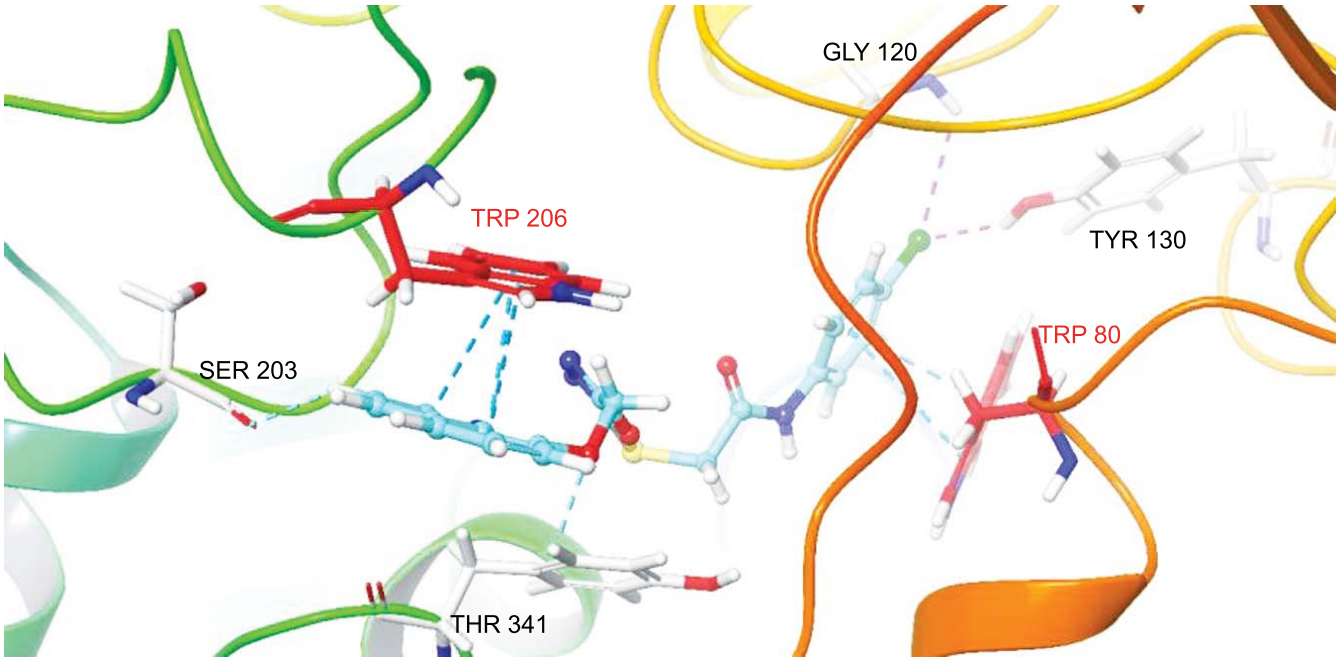

Fig. (6). 3D interactions of compound **5a** at the binding region (PBDID: 4EY7). (*A higher resolution / colour version of this figure is available in the electronic copy of the article*).

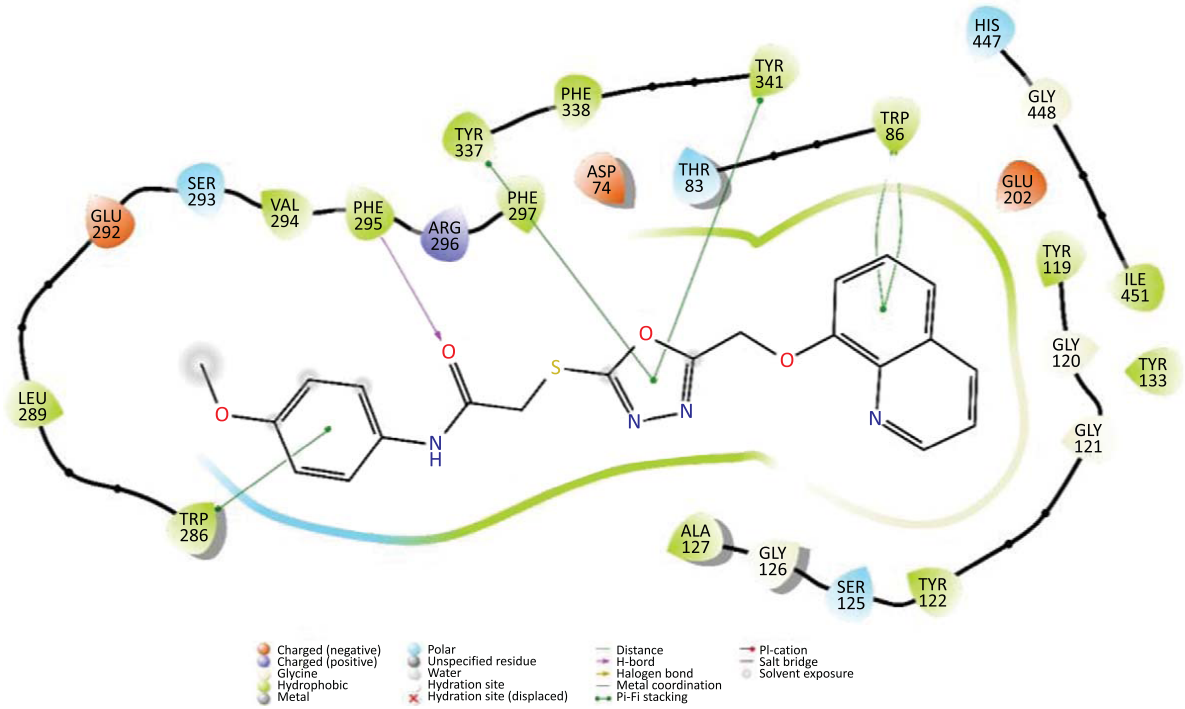

Fig (7). 2D interactions of compound **5c** at the binding region (PBDID: 4EY7). (*A higher resolution / colour version of this figure is available in the electronic copy of the article*).

Notably, the phenyl ring of the ligand also demonstrated two Ar-H interactions involving the phenyl H_2 and H_4 atoms, which interacted with Tyr341 and Arg296, respectively. Furthermore, an Ar-H interaction was observed between the quinoline C_2-H and Ser125. The overall binding conformation was further stabilized by a hydrogen bond formation between Phe295 and the carbonyl group of the ligand. These interactions collectively contribute to the favorable positioning of **5c** in the binding pocket of the enzyme (Fig. **8**).

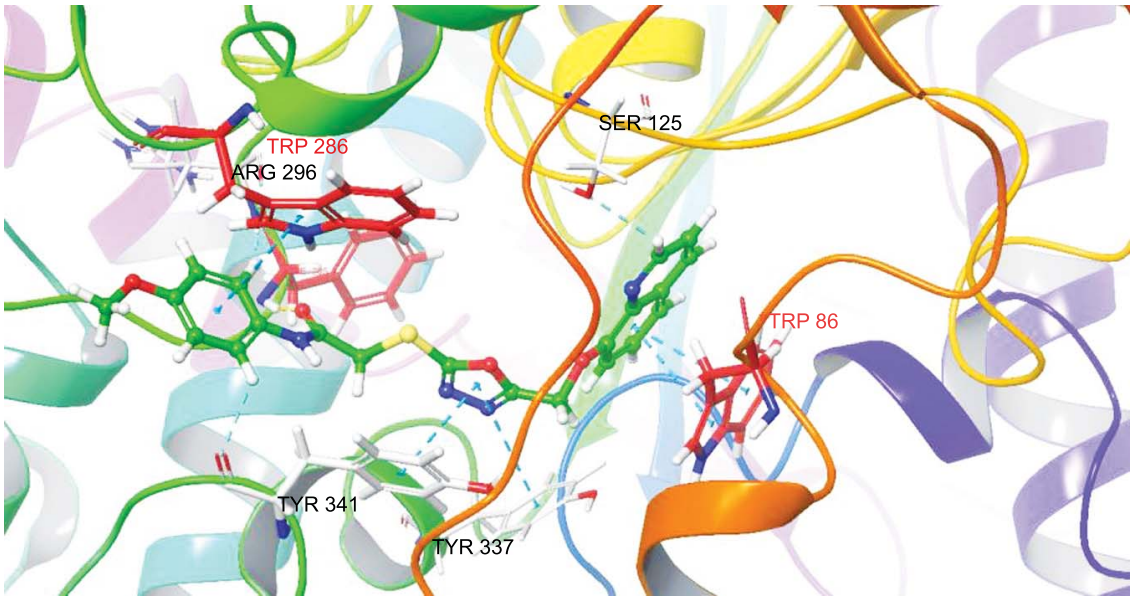

Fig. (8). 3D interactions of compound **5c** at the binding region (PBDID: 4EY7). (*A higher resolution / colour version of this figure is available in the electronic copy of the article*).

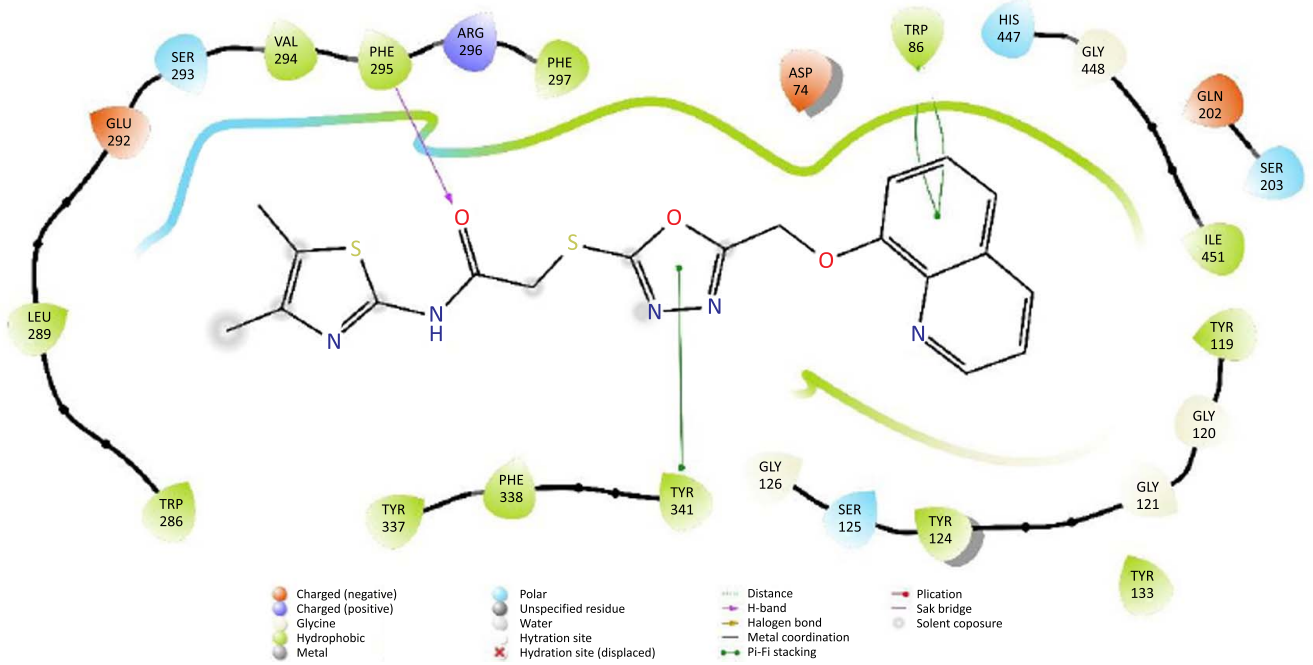

Fig. (9). 2D interactions of compound **6c** at the binding region (PBDID: 4EY7). (*A higher resolution / colour version of this figure is available in the electronic copy of the article*).

Blue carbons: compound **5c;** white carbons: binding site residues; cyan dashes: aromatic H-bond; blue dashes: π-π interaction; purple dashes: halogen interaction.

The interaction analysis of compound **6c** revealed several significant interactions with the active site. Notably, the quinoline ring of compound **6c** was found to interact with the indole residue of Trp86 through a π-π interaction. Additionally, a π-π interaction was observed between the oxadiazole ring of the ligand and Tyr341. Furthermore, the carbonyl moiety of the compound formed a hydrogen interaction with Phe295, further stabilizing its binding conformation within the active site (Fig. **9**). Moreover, two Ar-H interactions were detected: the quinoline C_3-H formed an interaction with Tyr133, while the quinoline C_6-H formed an interaction with His447. These interactions collectively contribute to the favorable positioning of compound **6c** within the binding pocket and may play a crucial role in its potential biological activity (Fig. **10**).

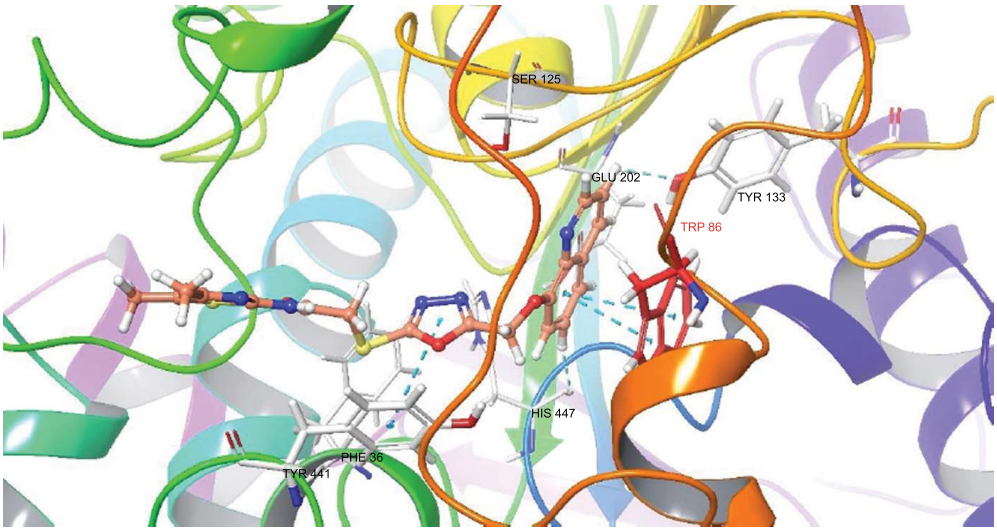

Fig. (10). 3D interactions of compound **6c** at the binding region (PBDID: 4EY7). (*A higher resolution / colour version of this figure is available in the electronic copy of the article*).

Blue carbons: compound **6c;** white carbons: binding site residues; cyan dashes: aromatic H-bond; blue dashes: π-π interaction; purple dashes: halogen interaction.

Based on the aforementioned findings, compounds **5a**, **5c,** and **6a** demonstrated the capability to interact with key amino acid residues Trp86 and Tyr341 in a manner comparable to the reference agent donepezil. Additionally, compounds **5a** and **5c**, characterized by the presence of 4-chloro and 4-methoxy substitutions on the acetanilide part, exhibited an essential interaction with Trp286 in the PAS. Both compounds **5c** and **6a** also demonstrated potential interactions with Phe295.

Furthermore, compound **6a** displayed elemental interactions with one component of the catalytic triad amino acids, His447. Importantly, all of these interactions were previously observed with donepezil, a potent acetylcholinesterase inhibitor. As a result, it is reasonable to anticipate that compounds **5a**, **5c**, and **6a** possess high inhibitory activity against acetylcholinesterase comparable to donepezil.

Furthermore, the study has uncovered that compounds **5a** and **6a** possess the ability to interact with Tyr133, which is involved in accommodating these compounds within the active site of acetylcholinesterase, akin to the interaction observed between huperzine A and AChE. This suggests that compounds **5a** and **6a** may share a similar binding mechanism with huperzine A, a known inhibitor of AChE [52].

Of particular interest, compound **5a** demonstrated the capability to bind with Gly120, which is an integral part of the glycine loop, forming the walls of the gorge alongside the catalytic serine. This interaction has the potential to influence the conformation of the glycine loop, which is recognized as a significant factor determining the geometry of the active center in huperzine and its inhibitory action. The binding of compound **5a** to Gly120 may, therefore, impact the structural arrangement and functionality of the glycine loop, further influencing the overall binding and inhibitory properties of the compound [53].

Additionally, it has been demonstrated that Tyr337 plays a crucial role in the interactions of compound **5c** with the enzyme, contributing to its positioning in a manner similar to huperzine A and tacrine. Furthermore, it is predicted that Ser125 contributes to stabilizing **5c** within the binding pocket, similar to the stabilization observed with aflatoxins in the catalytic anionic site (CAS). Moreover, the bonding with Arg296 is suggested to further strengthen the positioning of compound **5c** [54-56].

These findings indicate that the *in-vitro* enzyme study results align with the outcomes of the *in-silico* study. The observed interactions and positioning of compound **5c** in the active site of the enzyme, as supported by both experimental and computational approaches, provide valuable insights into its potential inhibitory activity against acetylcholinesterase.

3.6. Molecular Dynamics Simulation (MDS) Study Evaluation

Based on the molecular docking study results, we intended to perform MDS for the best candidate **5a** to evaluate the stability of the interactions with the enzyme acetylcholinesterase during the simulation time. Three plots were examined: the root mean square deviation (RMSD) *versus* time (ns), the root mean square fluctuation (RMSF) *versus* residue index, and the radius of gyration (Rg) *versus* time (ns) [57]. The minimal fluctuation observed in the Rg plot throughout the simulation course provided evidence of a high level of compactness in the protein and/or complex. The RMSD value of the protein was observed to alter by less than 1.80 Å, indicating the stability of the structure over the simulation course. Moreover, the fluctuation of the RMSD value of ligand fit on ligand has minimal changes, as shown in Fig. (**11**). The analysis of the RMSF plot has demonstrated the stability of the protein structure due to minimum fluctuation of the α-helix (red areas) and the β-strand (blue areas), as presented in Fig. (**12**). The loop region (white area) was also stabilized by interactions between the protein and the ligand. MDS data showed that the ligand **5a** interacted with the enzyme by forming hydrophobic interactions, H-bonds, and water bridges, as shown in Fig. (**13**). The hydrophobic interactions were formed with Tyr72, Val73, Leu76, Trp86, Tyr124, Trp286, Phe297, Tyr337, Phe338, and Tyr341. Meanwhile, the H-bonds were observed with Tyr124, Ser125, and Tyr337 amino acids. The water-mediated interactions were displayed with Tyr72, Asp74, Leu76, Thr83, Trp86, Gly121, Gly122, Tyr124, Ser125, Trp286, Ser293, Phe295, Arg296, Tyr337, Phe338, Tyr341, His447, and Tyr449 residues. Hydrophobic and water-mediated interactions were notably conserved during the entire simulation. The 2D plot of the minimum contact strength was generated to demonstrate the robustness of the interactions between the ligand and AChE throughout the entire simulation (Fig. **14**). All the rings in the compound (aromatic) quinoline, 1,3,4-oxadiazole, and phenyl rings participated in the interactions with the protein forming π-π interactions with Trp286, Tyr341, and Trp86 residues, as shown in Fig. (**14**) and Video **1**. The protein-ligand system was also further

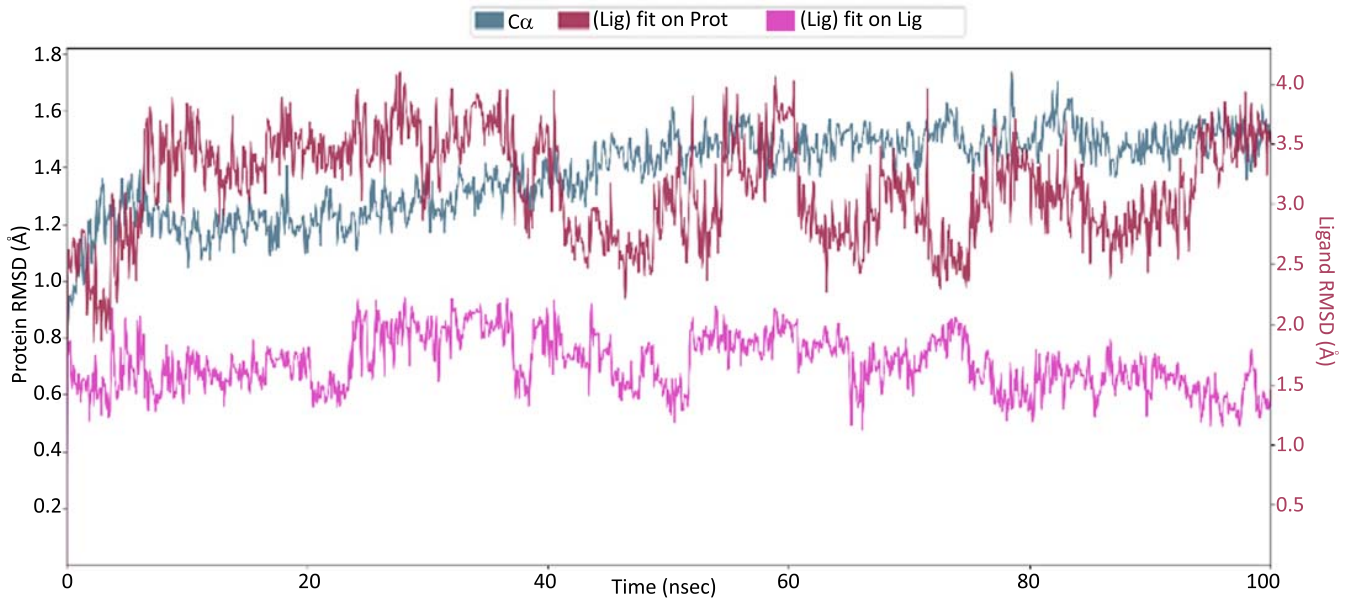

Fig. (11). Plot of root mean square deviation (RMSD); (Å)-time (ns). (*A higher resolution / colour version of this figure is available in the electronic copy of the article*).

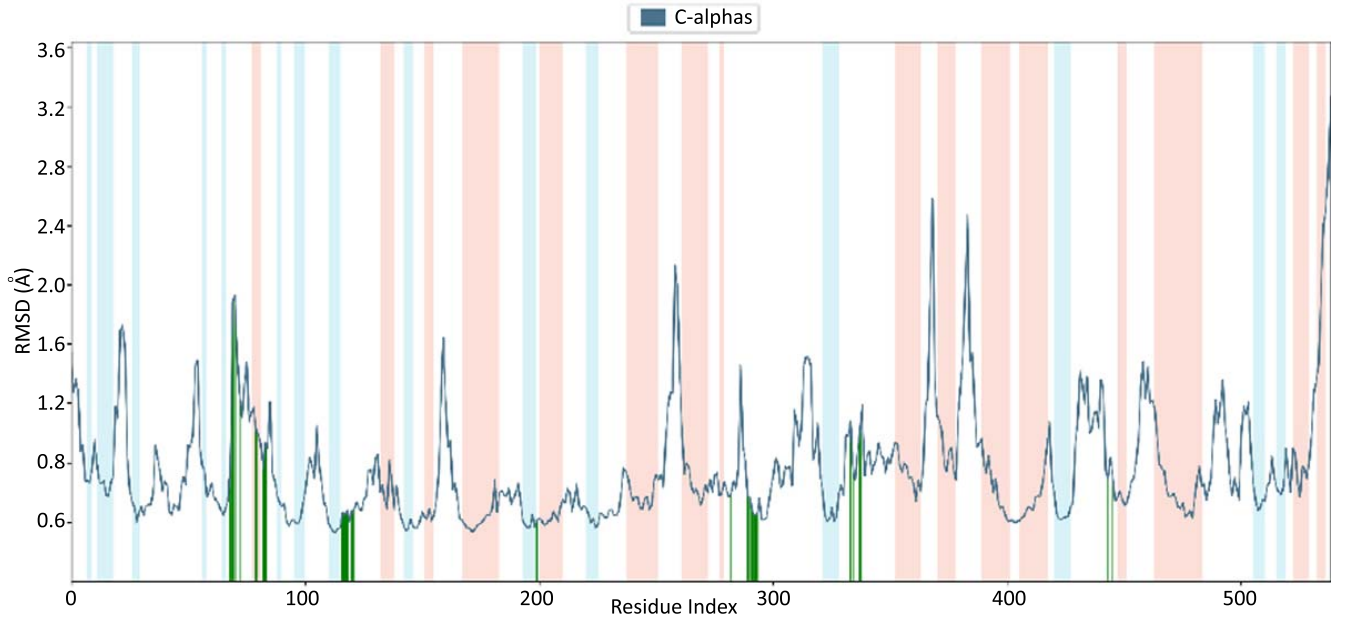

Fig. (12). Plot of root mean square fluctuation (RMSF)-residue index. The areas were represented in light red for the helices, light blue for the strands, and white for the loops. (*A higher resolution / colour version of this figure is available in the electronic copy of the article*).

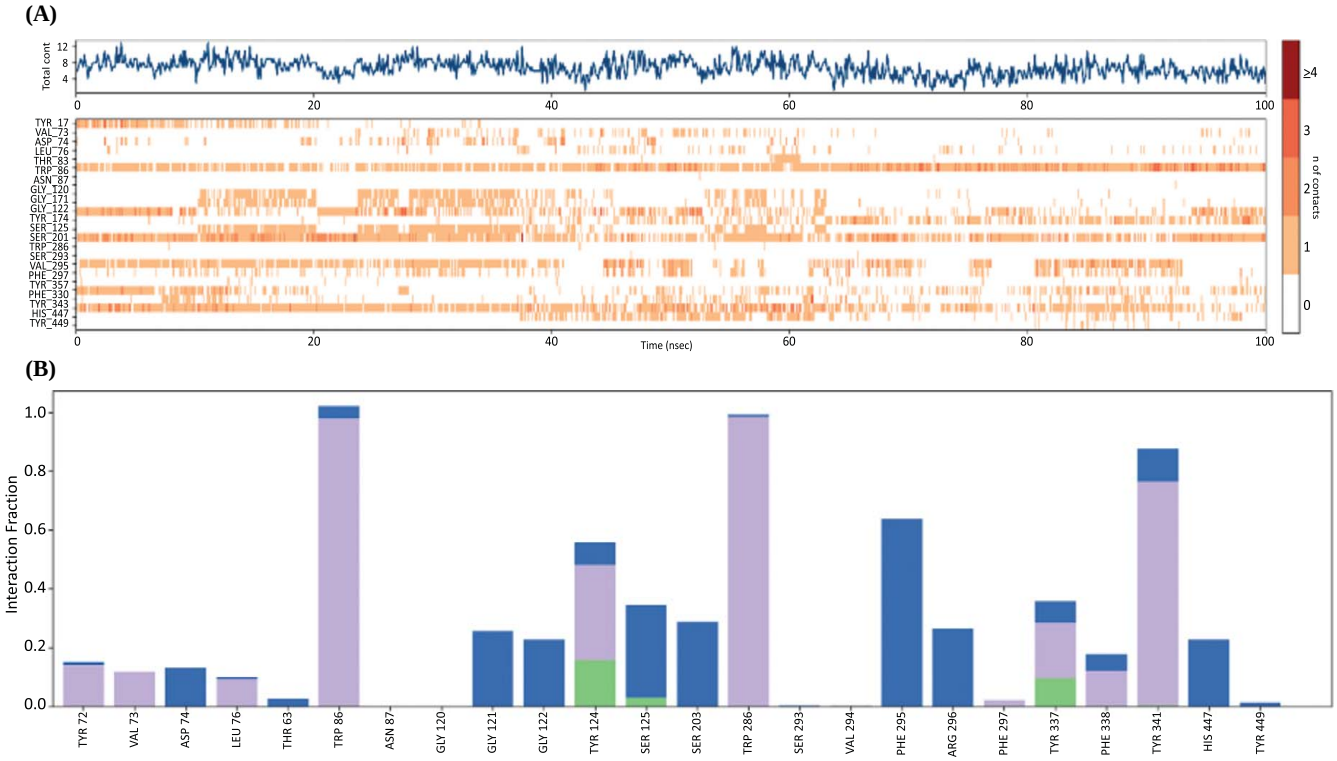

Fig. (13). (**A**) Number of interactions by residue during the simulation; (**B**) Plot of root mean square fluctuation-residue index. blue: water-mediated H-bond; green: H-bond; purple: hydrophobic interaction. (*A higher resolution / colour version of this figure is available in the electronic copy of the article*).

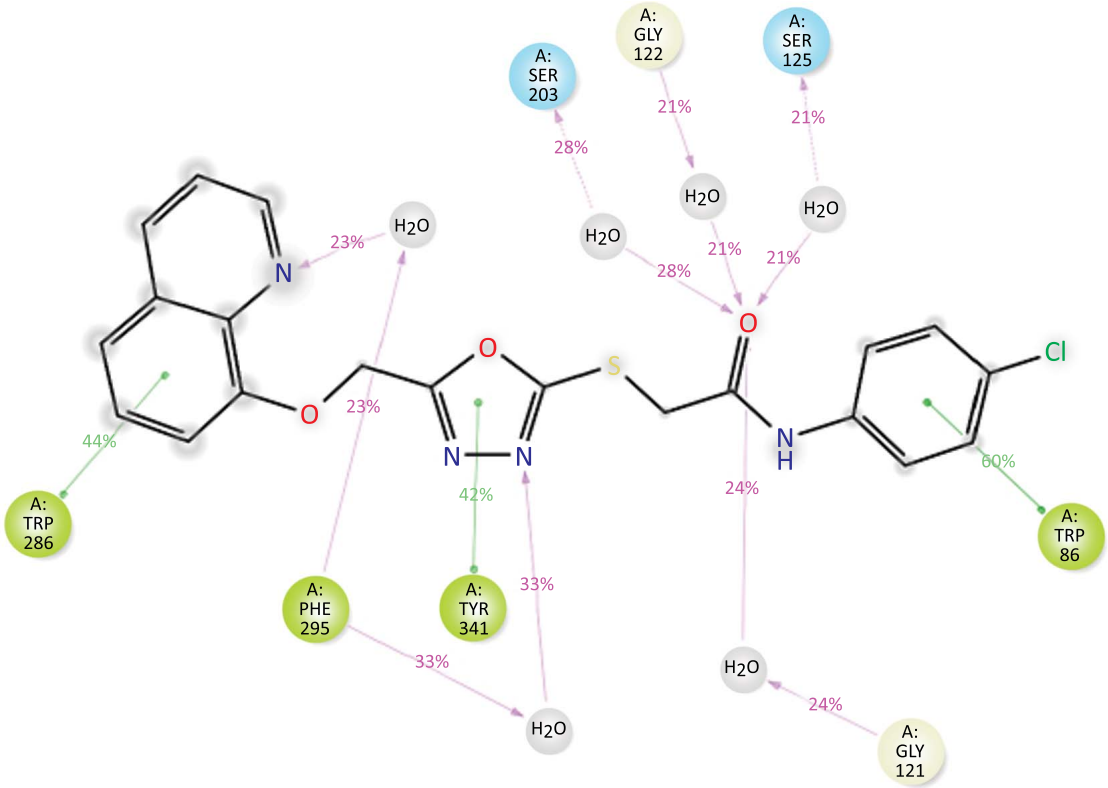

Fig. (14). Contact strength of **5a-**AchE complex. (*A higher resolution / colour version of this figure is available in the electronic copy of the article*).

stabilized by aromatic-H bonds (blue dashes) and aromatic-halogen interactions (purple dashes), which are shown in Video **2**. The chlorine atom in the para position of the phenyl ring displayed notable aromatic-halogen interaction with Gly120 throughout the simulation process. The oxygen of the amide group formed aromatic-H bonds with Gly121, Ser125, and Phe338. Meanwhile, the oxygen of oxadiazole rings participated as an aromatic-H bond acceptor with Ser125 and Phe338 residues. Moreover, the quinoline ring interaction with the binding site was further reinforced by aromatic-H bond formation with Ser293, Phe338, Tyr72, and Asp74 amino acids.

Both docking and MDS investigations provided evidence that **5a** effectively occupied the binding site of the enzyme, thereby elucidating the high inhibitory effect.

3.7. Structure-Activity Relationship Evaluation

The activity results and molecular docking studies provide insights into the preliminary structure-activity relationship of the compounds, as illustrated in Fig. (**15**). The presence of the quinoline ring is crucial for activity due to its ability to engage in hydrophobic interactions with key residues (Trp86 and Trp286) within the binding site of the acetylcholinesterase (AChE) enzyme [58]. The binding of the ligand within the active site was also enforced by the quinoline H-bonding with Ser293.

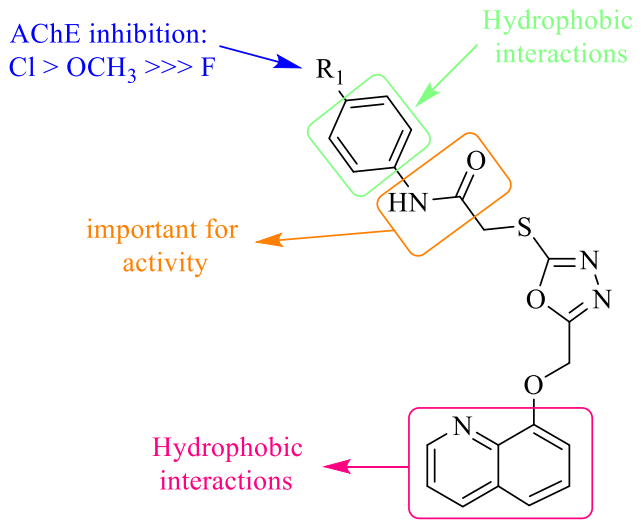

Fig. (15). Structure-activity relationship. (*A higher resolution / colour version of this figure is available in the electronic copy of the article*).

Noticeably, replacing the amide group between the thioether bridge and the aromatic ring (**5a-c**, **6a-c**) with a carbonyl group (**4a-d**) significantly decreases the potency of the compounds. Thus, the spacer length has an impact on the positioning of the compounds. The presence of a 4-substituted phenyl group contributes to notable inhibitory action through π-π interactions, whereas substituting this group with 4,5-substituted thiazole-2-yl leads to a pronounced decline in activity, highlighting the geometric size importance within the active site. Specific substitutions on the phenyl ring greatly influence activity; for instance, including 4-chloro and 4-methoxy groups leads to superior inhibition against AChE with IC_{50} of 0.033 μM and 0.096 μM, respectively. The highly potent potency produced by the chloro-substituted derivative might be explained by the "magic chloro" that has the ability to introduce aromatic-halogen interactions with crucial amino acids, affecting the conformation of the compound [59]. Moreover, the stable planar methoxy group at the para position was impacted by moderate inhibition, which resulted from its steric blocking properties and ability to fix the conformation of the ligand [60].

Moreover, introducing a fluorine atom at the para position dramatically reduced inhibitory activity (IC_{50}=0.177 μM). Although fluorine has higher electronegative properties, its smaller size compared to chlorine affected its ability to interact properly with the key residues within the active site. These findings emphasize the importance of specific structural features and substitutions in determining the inhibitory potency of the molecules against AChE, providing valuable insights for further optimization and development of potential AChE inhibitors.

CONCLUSION

In the pursuit of novel anticholinesterase and MAO inhibitors for the treatment of AD, a series of quinoline-oxadiazole hybrids were synthesized and assessed as potential candidates. Among the synthesized compounds, **5a**, **5c**, and **6a** displayed the most potent inhibitory activity against acetylcholinesterase with IC_{50} values of 0.033 μM, 0.096 μM, and 0.177 μM, respectively. However, none of the compounds exhibited notable inhibitory action against butyrylcholinesterase. Furthermore, the compounds were evaluated for their potential to inhibit the enzymes MAO-A and MAO-B. However, the inhibition percentages of the compounds were less than 50% at 10^{-3} and 10^{-4} concentrations.

The physicochemical properties of compounds **5a, 5c**, and **6a** were calculated and compared to those of donepezil. Additionally, molecular modeling and MDS methods were employed to study the binding modes and the interaction stability of the potent structures with AChE.

The higher potency of compound **5a** was attributed to its ability to interact with critical amino acid residues within the active site, similar to donepezil. Compound **5c** was found to retain the ability to bind with both the peripheral anionic site and the catalytic anionic site of the AChE enzyme. This dual inhibition of AChE by **5c** suggests its potential for an additional neuroprotective effect through reducing amyloid plaque deposition.

Overall, the structure-activity relationship of the compounds was elucidated based on the combination of activity results and molecular docking findings. These insights provide valuable information for the design and optimization of novel AChE inhibitors for the treatment of Alzheimer's disease.

AUTHORS' CONTRIBUTIONS

It is hereby acknowledged that all authors have accepted responsibility for the manuscript's content and consented to its submission. They have meticulously reviewed all results and unanimously approved the final version of the manuscript.

LIST OF ABBREVIATIONS

AD	=	Alzheimer's Disease
MAO-B	=	Monoamine Oxidase-B
AChE	=	Acetylcholinesterase
BuChE	=	Butyrylcholinesterase
SAR	=	Structure-activity Relationship
MDS	=	Molecular Dynamics Simulation
NFTs	=	Neurofibrillary Tangles

ETHICS APPROVAL AND CONSENT TO PARTICIPATE

Not applicable.

HUMAN AND ANIMAL RIGHTS

Not applicable.

CONSENT FOR PUBLICATION

Not applicable.

AVAILABILITY OF DATA AND MATERIALS

All data generated or analysed during this study are included in this published article.

FUNDING

This study was supported by Anadolu University within the scope of project no: 2204S032.

CONFLICT OF INTEREST

The authors declare no conflict of interest, financial or otherwise.

ACKNOWLEDGEMENTS

The study and supporting information are part of Master's thesis titled "New 1, 3, 4-Oxadiazole Derivatives and Investigation of their Biological Activity."

(Ref: Yurttaş, L. and Saffour, S., 2022. *New 1, 3, 4-oxadiazole derivatives and investigation of their biological activity* (Master's thesis, Anadolu Üniversitesi-Sağlık Bilimleri Enstitüsü)).

SUPPLEMENTARY MATERIAL

Supplementary material is available on the publisher's website along with the published article.

REFERENCES

[1] Weller, J.; Budson, A. Current understanding of Alzheimer's disease diagnosis and treatment. *F1000 Res.,* **2018**, *7*, 1161. http://dx.doi.org/10.12688/f1000research.14506.1

[2] Abeysinghe, A.A.D.T.; Deshapriya, R.D.U.S.; Udawatte, C. Alzheimer's disease; a review of the pathophysiological basis and therapeutic interventions. *Life Sci.,* **2020**, *256*, 117996. http://dx.doi.org/10.1016/j.lfs.2020.117996 PMID: 32585249

[3] Pohanka, M. Cholinesterases, a target of pharmacology and toxicology. *Biomed. Papers,* **2011**, *155*(3), 219-229. http://dx.doi.org/10.5507/bp.2011.036

[4] Saxena, M.; Dubey, R. Target enzyme in Alzheimer's disease: Acetylcholinesterase inhibitors. *Curr. Top. Med. Chem.,* **2019**, *19*(4), 264-275. http://dx.doi.org/10.2174/1568026619666190128125912 PMID: 30706815

[5] Singh, M.; Kaur, M.; Kukreja, H.; Chugh, R.; Silakari, O.; Singh, D. Acetylcholinesterase inhibitors as Alzheimer therapy: From nerve toxins to neuroprotection. *Eur. J. Med. Chem.,* **2013**, *70*, 165-188. http://dx.doi.org/10.1016/j.ejmech.2013.09.050 PMID: 24148993

[6] Li, Q.; He, S.; Chen, Y.; Feng, F.; Qu, W.; Sun, H. Donepezil-based multi-functional cholinesterase inhibitors for treatment of Alzheimer's disease. Vol. 158. *Eur. J. Med. Chem.,* **2018**.

[7] Diamant, S.; Podoly, E.; Friedler, A.; Ligumsky, H.; Livnah, O.; Soreq, H. Butyrylcholinesterase attenuates amyloid fibril formation *in vitro*. *Proc. Natl. Acad. Sci. USA,* **2006**, *103*(23), 8628-8633. http://dx.doi.org/10.1073/pnas.0602922103 PMID: 16731619

[8] Nordberg, A.; Ballard, C.; Bullock, R.; Darreh-Shori, T.; Somogyi, M. A review of butyrylcholinesterase as a therapeutic target in the treatment of Alzheimer's Disease. *Prim Care Companion CNS Disord,* **2013**, *15*(2), PCC.12r01412. http://dx.doi.org/10.4088/PCC.12r01412

[9] Bartorelli, L.; Giraldi, C.; Saccardo, M.; Cammarata, S.;

Bottini, G.; Fasanaro, A.M. Upgrade Study Group. Effects of switching from an AChE inhibitor to a dual AChE-BuChE inhibitor in patients with Alzheimer's disease. *Curr. Med. Res. Opin.,* **2005**, *21*(11), 1809-1818. http://dx.doi.org/10.1185/030079905X65655

[10] Zhao, T.; Ding, K.; Zhang, L.; Cheng, X.; Wang, C.; Wang, Z. Acetylcholinesterase and butyrylcholinesterase inhibitory activities of β -carboline and quinoline alkaloids derivatives from the plants of *Genus peganum*. *J. Chem.,* **2013**, *2013*, 1-6. http://dx.doi.org/10.1155/2013/717232

[11] Pflégr, V.; Štěpánková, Š.; Svrčková, K.; Švarcová, M.; Vinšová, J.; Krátký, M. 5-aryl-1,3,4-oxadiazol-2-amines decorated with long alkyl and their analogues: Synthesis, acetyl- and butyrylcholinesterase inhibition and docking study. *Pharmaceuticals,* **2022**, *15*(4), 400. http://dx.doi.org/10.3390/ph15040400

[12] Hampel, H.; Mesulam, M.M.; Cuello, A.C.; Farlow, M.R.; Giacobini, E.; Grossberg, G.T.; Khachaturian, A.S.; Vergallo, A.; Cavedo, E.; Snyder, P.J.; Khachaturian, Z.S. The cholinergic system in the pathophysiology and treatment of Alzheimer's disease. *Brain,* **2018**, *141*(7), 1917-1933. http://dx.doi.org/10.1093/brain/awy132 PMID: 29850777

[13] Hollmann, P. Update: FDA approval of Biogen's aducanumab. *Geriatr. Nurs.,* **2022**, *43*, 318-319. http://dx.doi.org/10.1016/j.gerinurse.2021.12.018 PMID: 34996638

[14] Youdim, M.B.H.; Edmondson, D.; Tipton, K.F. The therapeutic potential of monoamine oxidase inhibitors. *Nat. Rev. Neurosci.,* **2006**, *7*(4), 295-309. http://dx.doi.org/10.1038/nrn1883 PMID: 16552415

[15] Riederer, P.; Danielczyk, W.; Grünblatt, E. Monoamine oxidase-B inhibition in Alzheimer's disease. *Neurotoxicol,* **2004**, *25*(1-2), 271-277. http://dx.doi.org/10.1016/S0161-813X(03)00106-2

[16] Cai, Z. Monoamine oxidase inhibitors: Promising therapeutic agents for Alzheimer's disease (Review). *Mol. Med. Rep.,* **2014**, *9*(5), 1533-1541. http://dx.doi.org/10.3892/mmr.2014.2040 PMID: 24626484

[17] Pohanka, M. Acetylcholinesterase inhibitors: a patent review (2008–present). *Expert Opin. Ther. Pat.,* **2012**, *22*(8), 871-886. http://dx.doi.org/10.1517/13543776.2012.701620 PMID: 22768972

[18] AL-Sharabi, AA. Evren AE, Sağlık BN, Yurttaş L. Synthesis, characterization, molecular docking and molecular dynamics simulations of novel 2,5-disubstituted-1,3,4-thiadiazole derivatives as potential cholinesterase/monoamine oxidase dual inhibitors for Alzheimer's disease. *J. Biomol. Struct. Dyn.,* **2023**, 1-19.

[19] Dorababu, A. Promising heterocycle-based scaffolds in recent (2019–2021) anti-Alzheimer's drug design and discovery. *Eur. J. Pharmacol.,* **2022**, *920*, 174847. http://dx.doi.org/10.1016/j.ejphar.2022.174847 PMID: 35218718

[20] Boström, J.; Hogner, A.; Llinà, A.; Wellner, E.; Plowright, A.T. Oxadiazoles in medicinal chemistry. *J. Med. Chem.,* **2011**, *55*(5), 1817-1830.

[21] Saha, R.; Tanwar, O.; Marella, A.; Mumtaz Alam, M.; Akhter, M. Recent updates on biological activities of oxadiazoles. *Mini Rev. Med. Chem.,* **2013**, *13*(7), 1027-1046. http://dx.doi.org/10.2174/1389557511313070007 PMID: 22512577

[22] Wen, M.W.; Sha, J.S.; Xiao, W.; Dong, W.X.; Quan, M.W. Synthesis and biological evaluation of benzothiazol-based 1,3,4-oxadiazole derivatives as amyloid β-targeted compounds against Alzheimer's disease. *Monatsh Chem.,* **2017**, *148*(10), 1807-1815.

[23] Ibrar, A.; Khan, A.; Ali, M.; Sarwar, R.; Mehsud, S.; Farooq, U.; Halimi, S.M.A.; Khan, I.; Al-Harrasi, A. Combined *in vitro* and *in silico* studies for the anticholinesterase activity and pharmacokinetics of coumarinyl thiazoles and oxadiazoles. *Front Chem.,* **2018**, *6*(MAR), 61. http://dx.doi.org/10.3389/fchem.2018.00061 PMID: 29632858

[24] George, N.; Sabahi, B.A.; AbuKhader, M.; Balushi, K.A.; Akhtar, M.J.; Khan, S.A. Design, synthesis and *in vitro* biological activities of coumarin linked 1,3,4-oxadiazole hybrids as potential multi-target directed anti-Alzheimer agents. *J. King Saud Univ. Sci.,* **2022**, *34*(4), 101977. http://dx.doi.org/10.1016/j.jksus.2022.101977

[25] Tripathi, A.; Choubey, P.K.; Sharma, P.; Seth, A.; Saraf, P.; Shrivastava, S.K. Design, synthesis, and biological evaluation of ferulic acid based 1,3,4-oxadiazole hybrids as multifunctional therapeutics for the treatment of Alzheimer's disease. *Bioorg. Chem.,* **2020**, *95*, 103506. http://dx.doi.org/10.1016/j.bioorg.2019.103506 PMID: 31887472

[26] Choubey, P.K.; Tripathi, A.; Tripathi, M.K.; Seth, A.; Shrivastava, S.K. Design, synthesis, and evaluation of N-benzylpyrrolidine and 1,3,4-oxadiazole as multitargeted hybrids for the treatment of Alzheimer's disease. *Bioorg. Chem.,* **2021**, *111*, 104922. http://dx.doi.org/10.1016/j.bioorg.2021.104922 PMID: 33945941

[27] Tok, F.; Uğraş, Z.; Sağlık, B.N.; Özkay, Y.; Kaplancıklı, Z.A.; Koçyiğit-Kaymakçıoğlu, B. Novel 2,5-disubstituted-1,3,4-oxadiazole derivatives as MAO-B inhibitors: Synthesis, biological evaluation and molecular modeling studies. *Bioorg. Chem.,* **2021**, *112*, 104917. http://dx.doi.org/10.1016/j.bioorg.2021.104917 PMID: 33932769

[28] Karabelyov, V.; Kondeva-Burdina, M.; Angelova, V.T. Synthetic approaches to unsymmetrical 2,5-disubstituted 1,3,4-oxadiazoles and their MAO-B inhibitory activity. A review. *Bioorg. Med. Chem.,* **2021**, *29*, 115888. http://dx.doi.org/10.1016/j.bmc.2020.115888 PMID: 33360082

[29] Sharma, P.; Tripathi, A.; Tripathi, P.N.; Singh, S.S.; Singh, S.P.; Shrivastava, S.K. Novel molecular hybrids of *N* -benzylpiperidine and 1,3,4-oxadiazole as multitargeted therapeutics to treat alzheimer's disease. *ACS Chem. Neurosci.,* **2019**, *10*(10), 4361-4384. http://dx.doi.org/10.1021/acschemneuro.9b00430 PMID: 31491074

[30] Marella, A.; Tanwar, O.P.; Saha, R.; Ali, M.R.; Srivastava, S.; Akhter, M.; Shaquiquzzaman, M.; Alam, M.M. Quinoline: A versatile heterocyclic. *Saudi Pharm. J.,* **2013**, *21*(1), 1-12. http://dx.doi.org/10.1016/j.jsps.2012.03.002

[31] Yadav, P.; Shah, K. Quinolines, a perpetual, multipurpose scaffold in medicinal chemistry. *Bioorg. Chem.,* **2021**, *109*, 104639. http://dx.doi.org/10.1016/j.bioorg.2021.104639 PMID: 33618829

[32] Bowroju, S.K.; Mainali, N.; Ayyadevara, S.; Penthala, N.R.; Krishnamachari, S.; Kakraba, S.; Reis, R.J.S.; Crooks, P.A. Design and synthesis of novel hybrid 8-hydroxy quinoline-indole derivatives as inhibitors of Aβ self-

-aggregation and metal chelation-induced Aβ aggregation. *Molecules,* **2020**, *25*(16), 3610. http://dx.doi.org/10.3390/molecules25163610 PMID: 32784464

[33] Mantoani, S.P.; Chierrito, T.P.C.; Vilela, A.F.L.; Cardoso, C.L.; Martínez, A.; Carvalho, I. Novel triazole-quinoline derivatives as selective dual binding site acetylcholinesterase inhibitors. *Molecules.,* **2016**, *21*(2), 193. http://dx.doi.org/10.3390/molecules21020193

[34] Shah, M.S.; Najam-ul-Haq, M.; Shah, H.S.; Farooq Rizvi, S.U.; Iqbal, J. Quinoline containing chalcone derivatives as cholinesterase inhibitors and their *in silico* modeling studies. *Comput. Biol. Chem.,* **2018**, *76*, 310-317. http://dx.doi.org/10.1016/j.compbiolchem.2018.08.003 PMID: 30142564

[35] Adlard, P.A.; Cherny, R.A.; Finkelstein, D.I.; Gautier, E.; Robb, E.; Cortes, M.; Volitakis, I.; Liu, X.; Smith, J.P.; Perez, K.; Laughton, K.; Li, Q.X.; Charman, S.A.; Nicolazzo, J.A.; Wilkins, S.; Deleva, K.; Lynch, T.; Kok, G.; Ritchie, C.W.; Tanzi, R.E.; Cappai, R.; Masters, C.L.; Barnham, K.J.; Bush, A.I. Rapid restoration of cognition in Alzheimer's transgenic mice with 8-hydroxy quinoline analogs is associated with decreased interstitial Abeta. *Neuron,* **2008**, *59*(1), 43-55. http://dx.doi.org/10.1016/j.neuron.2008.06.018 PMID: 18614028

[36] Barth, A.; Vogt, A.G.; dos Reis, A.S.; Pinz, M.P.; Krüger, R.; Domingues, W.B.; Alves, D.; Campos, V.F.; Pinton, S.; Paroul, N.; Wilhelm, E.A.; Luchese, C. 7-Chloro-4-(bhenylselanyl) quinoline with memory enhancer action in aging rats: modulation of neuroplasticity, acetylcholinesterase activity, and cholesterol levels. *Mol. Neurobiol.,* **2019**, *56*(9), 6398-6408. http://dx.doi.org/10.1007/s12035-019-1530-5 PMID: 30805835

[37] Sang, Z.; Pan, W.; Wang, K.; Ma, Q.; Yu, L.; Liu, W. Design, synthesis and biological evaluation of 3,4-dihydro-2(1 H)-quinoline- O -alkylamine derivatives as new multipotent cholinesterase/monoamine oxidase inhibitors for the treatment of Alzheimer's disease. *Bioorg. Med. Chem.,* **2017**, *25*(12), 3006-3017. http://dx.doi.org/10.1016/j.bmc.2017.03.070 PMID: 28487125

[38] Zaib, S.; Munir, R.; Younas, M.T.; Kausar, N.; Ibrar, A.; Aqsa, S.; Shahid, N.; Asif, T.T.; Alsaab, H.O.; Khan, I. Hybrid quinoline-thiosemicarbazone therapeutics as a new treatment opportunity for Alzheimer's disease-synthesis, *in vitro* cholinesterase inhibitory potential and computational modeling analysis. *Molecules,* **2021**, *26*(21), 6573. http://dx.doi.org/10.3390/molecules26216573 PMID: 34770983

[39] Duarte, Y.; Fonseca, A.; Gutiérrez, M.; Adasme-Carreño, F.; Muñoz-Gutierrez, C.; Alzate-Morales, J.; Santana, L.; Uriarte, E.; Álvarez, R.; Matos, M.J. Novel coumarin-quinoline hybrids: design of multitarget compounds for Alzheimer's disease. *ChemistrySelect,* **2019**, *4*(2), 551-558. http://dx.doi.org/10.1002/slct.201803222

[40] Yurttaş, L.; Kubilay, A.; Evren, A.E.; Kısacık, İ.; Karaca Gençer, H. Synthesis of some novel 3,4,5-trisubstituted triazole derivatives bearing quinoline ring and evaluation of their antimicrobial activity. *Phosphorus Sulfur Silicon Relat. Elem.,* **2020**, *195*(9), 767-773. http://dx.doi.org/10.1080/10426507.2020.1756808

[41] Yurttaş, L.; Bülbül, E.F.; Tekinkoca, S.; Demirayak, Ş. Antimicrobial activity evaluation of new 1,3,4-oxadiazole derivatives. *ACTA Pharmaceutica Sciencia,* **2017**, *55*(2), 45. http://dx.doi.org/10.23893/1307-2080.APS.05511

[42] Kaplancikli, Z.A.; Yurttaş, L.; Özdemir, A.; Turan-Zitouni, G.; İşcan, G.; Akalın, G.; Abu Mohsen, U. Synthesis, anticandidal activity and cytotoxicity of some tetrazole derivatives. *J. Enzyme Inhib. Med. Chem.,* **2014**, *29*(1), 43-48. http://dx.doi.org/10.3109/14756366.2012.752363 PMID: 23323990

[43] Yurttaş, L.; Özkay, Y.; Akalin-Çiftçi, G.; Ulusoylar-Yildirim, Ş. Synthesis and anticancer activity evaluation of N-[4-(2-methylthiazol-4-yl)phenyl]acetamide derivatives containing (benz)azole moiety. *J. Enzyme. Inhib. Med. Chem.,* **2014**, *29*(2), 175-184. http://dx.doi.org/10.3109/14756366.2013.763253

[44] Zheng, Q.Z.; Zhang, X.M.; Xu, Y.; Cheng, K.; Jiao, Q.C.; Zhu, H.L. Synthesis, biological evaluation, and molecular docking studies of 2-chloropyridine derivatives possessing 1,3,4-oxadiazole moiety as potential antitumor agents. *Bioorg. Med. Chem.,* **2010**, *18*(22), 7836-7841. http://dx.doi.org/10.1016/j.bmc.2010.09.051 PMID: 20947362

[45] Demirayak, Ş.; Şahin, Z.; Ertaş, M.; Bülbül, E.F.; Bender, C.; Biltekin, S.N.; Berk, B.; Sağlık, B.N.; Levent, S.; Yurttaş, L. Novel thiazole-piperazine derivatives as potential cholinesterase inhibitors. *J. Heterocycl. Chem.,* **2019**, *56*(12), 3370-3386. http://dx.doi.org/10.1002/jhet.3734

[46] Sağlık, B.N.; Ilgın, S.; Özkay, Y. Synthesis of new donepezil analogues and investigation of their effects on cholinesterase enzymes. *Eur. J. Med. Chem.,* **2016**, *124*, 1026-1040. http://dx.doi.org/10.1016/j.ejmech.2016.10.042 PMID: 27783974

[47] Osmaniye, D.; Evren, A.E.; Sağlık, B.N.; Levent, S.; Özkay, Y.; Kaplancıklı, Z.A. Design, synthesis, biological activity, molecular docking, and molecular dynamics of novel benzimidazole derivatives as potential AChE/-MAO-B dual inhibitors. *Arch. Pharm. (Weinheim),* **2022**, *355*(3), 2100450. http://dx.doi.org/10.1002/ardp.202100450 PMID: 34931332

[48] Sağlık, B.N.; Kaya Çavuşoğlu, B.; Osmaniye, D.; Levent, S.; Acar Çevik, U.; Ilgın, S.; Özkay, Y.; Kaplancıklı, Z.A.; Öztürk, Y. *In vitro* and *in silico* evaluation of new thiazole compounds as monoamine oxidase inhibitors. *Bioorg. Chem.,* **2019**, *85*, 97-108. http://dx.doi.org/10.1016/j.bioorg.2018.12.019 PMID: 30605888

[49] Daina, A.; Michielin, O.; Zoete, V. SwissADME: a free web tool to evaluate pharmacokinetics, drug-likeness and medicinal chemistry friendliness of small molecules. *Sci. Rep.,* **2017**, *7*(1), 42717. http://dx.doi.org/10.1038/srep42717 PMID: 28256516

[50] Cheung, J.; Rudolph, M.J.; Burshteyn, F.; Cassidy, M.S.; Gary, E.N.; Love, J.; Franklin, M.C.; Height, J.J. Structures of human acetylcholinesterase in complex with pharmacologically important ligands. *J. Med. Chem.,* **2012**, *55*(22), 10282-10286. http://dx.doi.org/10.1021/jm300871x PMID: 23035744

[51] Evren, A.E.; Nuha, D.; Dawbaa, S.; Sağlık, B.N.; Yurttaş, L. Synthesis of novel thiazolyl hydrazone derivatives as potent dual monoamine oxidase-aromatase inhibitors. *Eur. J.*

Med. Chem., **2022**, *229*, 114097.
http://dx.doi.org/10.1016/j.ejmech.2021.114097 PMID: 34998057

[52] Ariel, N.; Ordentlich, A.; Barak, D.; Bino, T.; Velan, B.; Shafferman, A. The 'aromatic patch' of three proximal residues in the human acetylcholinesterase active centre allows for versatile interaction modes with inhibitors. *Biochem. J.,* **1998**, *335*(1), 95-102.
http://dx.doi.org/10.1042/bj3350095 PMID: 9742217

[53] Ordentlich, A.; Barak, D.; Kronman, C.; Flashner, Y.; Leitner, M.; Segall, Y.; Ariel, N.; Cohen, S.; Velan, B.; Shafferman, A. Dissection of the human acetylcholinesterase active center determinants of substrate specificity. Identification of residues constituting the anionic site, the hydrophobic site, and the acyl pocket. *J. Biol. Chem.,* **1993**, *268*(23), 17083-17095.
http://dx.doi.org/10.1016/S0021-9258(19)85305-X PMID: 8349597

[54] De Almeida, J.S.F.D.; Dolezal, R.; Krejcar, O.; Kuca, K.; Musilek, K.; Jun, D.; França, T.C.C. Molecular modeling studies on the interactions of aflatoxin B1 and its metabolites with human acetylcholinesterase. Part II: Interactions with the catalytic anionic site (CAS). *Toxins (Basel),* **2018**, *10*(10), 389.
http://dx.doi.org/10.3390/toxins10100389 PMID: 30257474

[55] Sahin, Z.; Ertas, M.; Bender, C.; Bülbül, E.F.; Berk, B.; Biltekin, S.N.; Yurttaş, L.; Demirayak, Ş. Thiazole-substituted benzoylpiperazine derivatives as acetylcholinesterase inhibitors. *Drug Dev. Res.,* **2018**, *79*(8), 406-425.
http://dx.doi.org/10.1002/ddr.21481 PMID: 30343499

[56] Singh, Y.P.; Tej, G.N.V.C.; Pandey, A.; Priya, K.; Pandey, P.; Shankar, G.; Nayak, P.K.; Rai, G.; Chittiboyina, A.G.; Doerksen, R.J.; Vishwakarma, S.; Modi, G. Design, synthesis and biological evaluation of novel naturally-inspired multifunctional molecules for the management of Alzheimer's disease. *Eur. J. Med. Chem.,* **2020**, *198*, 112257.
http://dx.doi.org/10.1016/j.ejmech.2020.112257 PMID: 32375073

[57] Durmaz, Ş.; Evren, A.E.; Sağlık, B.N.; Yurttaş, L.; Tay, N.F. Synthesis, anticholinesterase activity, molecular docking, and molecular dynamic simulation studies of 1,3,4-oxadiazole derivatives. *Arch. Pharm. (Weinheim),* **2022**, *355*(11), 2200294.
http://dx.doi.org/10.1002/ardp.202200294 PMID: 35972839

[58] Peitzika, S.C.; Pontiki, E. A review on recent approaches on molecular docking studies of novel compounds targeting acetylcholinesterase in Alzheimer disease. *Molecules,* **2023**, *28*(3), 1084.
http://dx.doi.org/10.3390/molecules28031084 PMID: 36770750

[59] Chiodi, D.; Ishihara, Y. "Magic Chloro": Profound effects of the chlorine atom in drug discovery. *J. Med. Chem.,* **2023**, *66*(8), 5305-5331.
http://dx.doi.org/10.1021/acs.jmedchem.2c02015 PMID: 37014977

[60] Chiodi, D.; Ishihara, Y. The role of the methoxy group in approved drugs. *Eur. J. Med. Chem.,* **2024**, *273*(116364), 116364.
http://dx.doi.org/10.1016/j.ejmech.2024.116364 PMID: 38781921